

# Non-linear vorticity upsurge in Burgers flow

BY F. LAM

We demonstrate that numerical solutions of Burgers' equation can be obtained by a scale-totality algorithm for fluids of small viscosity (down to one billionth). Two sets of initial data, modelling simple shears and wall boundary layers, are chosen for our computations. Most of the solutions are carried out well into the fully turbulent regime over finely-resolved scales in space and in time. It is found that an abrupt spatio-temporal concentration in shear constitutes an essential part during the flow evolution. The vorticity surge has been instigated by the non-linearity complying with instantaneous enstrophy production while *ad hoc* disturbances play no role in the process. In particular, the present method *predicts* the precipitous vorticity re-distribution and accumulation, predominantly over localised regions of minute dimension. The growth rate depends on viscosity and is a strong function of initial data. Nevertheless, the long-time energy decay is history-independent and is inversely proportional to time. Our results provide direct evidence of the vorticity proliferation embedded in the equations of motion. The non-linear intensification is a robust feature and is ultimately responsible for the drastic succession in boundary layer profiles over the intrinsic laminar-turbulent transition (Schubauer and Klebanoff 1955). The dynamical inception of turbulence can be decrypted by solving the full time-dependent Navier-Stokes equations which ascribe no instability stages.

**Keywords:** Navier-Stokes Regularity; Burgers equation; Viscosity; Vorticity; Laminar-turbulent Transition; Non-linearity; Shock; Turbulence Decay

## 1. Introduction

It has been long known that fluid motions start from streamlined laminar state, undergo *laminar-turbulent transition* and evolve into randomly fluctuating poly-scaled turbulence (Reynolds 1883; Taylor 1923; Schubauer & Skramstad 1947). In the Eulerian description of the motion of an incompressible, homogeneous Newtonian fluid, the Navier-Stokes equations of motion and the continuity read

$$\partial \mathbf{u} / \partial t + (\mathbf{u} \cdot \nabla) \mathbf{u} = \nu \Delta \mathbf{u} - \rho^{-1} \nabla p, \quad \nabla \cdot \mathbf{u} = 0, \quad (1.1)$$

where vector  $\mathbf{u} = \mathbf{u}(\mathbf{x}, t)$  are the velocity having the components  $(\mathbf{u}_1, \mathbf{u}_2, \mathbf{u}_3)$ , the scalar quantity  $p = p(\mathbf{x}, t)$  denotes the pressure,  $\mathbf{x} = (\mathbf{x}_1, \mathbf{x}_2, \mathbf{x}_3)$  the space variable, and  $\Delta$  the Laplacian. The kinematic viscosity is  $\nu = \mu / \rho$ , where  $\rho$  and  $\mu$  are the density and viscosity respectively. We are interested in the initial-boundary value problem of (1.1) from given data of finite energy

$$\mathbf{u}(\mathbf{x}, t=0) = \mathbf{u}_0(\mathbf{x}) \in C_c^\infty(\Omega), \quad (1.2)$$

and  $\nabla \cdot \mathbf{u}_0 = 0$ . The no-slip boundary condition applies on the (smooth) boundary of the domain  $\Omega$

$$\mathbf{u}(\mathbf{x}, t) = 0 \quad \forall \mathbf{x} \in \partial \Omega. \quad (1.3)$$

Taking divergence of (1.1) and utilising the continuity, we derive a Poisson equation for the pressure

$$\Delta p(\mathbf{x}) = -\rho \sum_{i,j=1}^3 \left( \frac{\partial \mathbf{u}_j}{\partial \mathbf{x}_i} \frac{\partial \mathbf{u}_i}{\partial \mathbf{x}_j} \right)(\mathbf{x}) \quad (1.4)$$

whose solution is well-known. Vorticity is a physical (vector) quantity,  $\omega = \nabla \times \mathbf{u}$  and is related to the angular momentum in flow motions. The vorticity equation is

$$\partial \omega / \partial t - \nu \Delta \omega = (\omega \cdot \nabla) \mathbf{u} - (\mathbf{u} \cdot \nabla) \omega. \quad (1.5)$$

The vorticity field inherits the solenoidal property of (1.1)  $\nabla \cdot \omega = 0$ . At every given instant of time, we recover the velocity from the di-vorticity from the Biot-Savart relation

$$\mathbf{u}(\mathbf{x}) = \Delta^{-1}(\nabla \times \omega), \quad (1.6)$$

where  $\Delta^{-1}$  stands for the Laplacian inverse in  $\Omega$  satisfying (1.3). This is an elliptic relation, just like the solution of (1.4). Neither contains time information.

To solve dynamic problems for fluid motions, we may tackle either (1.1)-(1.4) or (1.5)-(1.6) with appropriate initial and boundary data. In theory, each set of the equations defines a *parabolic-elliptic* system by the assumption of incompressibility. The Navier-Stokes equations describe the mean velocity as well as pressure (in the sense of ensemble averages) and do not model the random fluctuations in turbulent motions. For practical purposes, it is precisely the motive underlying the continuum hypothesis where only mean flow quantities, such as skin friction and average energy dissipation increase over transition, really matter.

The study of the transitional dynamics is to address the mechanism of *en masse* scale initiation by the term  $(\mathbf{u} \cdot \nabla) \mathbf{u}$ . Consequently, the causality of external disturbances on flow development is of secondary importance; the effects of extraneous forcing can only be well-quantified once the intrinsic transition has been understood. In the present paper, an effort is made to analyse the non-linear dynamics by solving Burgers' equation numerically. We shall present our numerical evidence for the intrinsic process in small-viscosity flows. By examining the solutions, we anticipate to distinguish the hallmarks of the transition process as identified from experiments.

## 2. Burgers' equation and mathematics of turbulence

Burgers' equation refers to the parabolic equation in one space dimension (Burgers 1948):

$$\frac{\partial u}{\partial t} - \nu \frac{\partial^2 u}{\partial x^2} = -u \frac{\partial u}{\partial x}. \quad (2.1)$$

We seek its solutions subject to initial-boundary conditions,

$$u(x, t = 0) = u_0(x), \quad \text{and} \quad u(0, t) = u(1, t) = 0. \quad (2.2)$$

Two initial data examined in the present paper are given by

$$u_0(x) = A_0 \sin(\pi x), \quad (2.3)$$

which evolves into a boundary layer near  $x = 1$  for constant intensity  $A_0 > 0$ , and

$$u_0(x) = A_0 \sin(2\pi x), \quad (2.4)$$

whose time-wise development resembles the formation of a shear layer or a standing saw-tooth shock in the vicinity of  $x = 0.5$ .

In many textbooks on differential equations, the following example is often cited to illustrate the existence of blow-up solutions. Let  $u=u(t)$  be governed by the ordinary differential equation

$$du/dt = u^2, \quad u(t=0) = u_0.$$

By means of substitution  $u = 1/v$ , the solution is found to be  $u(t) = u_0/(1 - u_0 t)$  which blows up at  $t = 1/u_0$  for positive initial data. For finite  $t < 1/u_0$ , the solution is regular. Taking  $u$  as velocity, the blow-up scenario contradicts the laws of thermodynamics. We may blame the negligence of certain dissipation in our model. In part, the contradiction is due to our mathematical analysis. Consider the motion in time reversal (or adjoint in a sense),  $t \rightarrow -t$ . Now the blow-up solution becomes  $u(t) = u_0/(1 + u_0 t)$  which is globally regular for the identical positive data. The first law suggests that the blow-up option must be discarded, in the same way as choosing exponentially damped eigen-states. Similar principles hold for equations containing a cubic non-linearity  $\pm u^3$ . The singularity scenarios violating the thermodynamic principles have no justifications in classical physics.

The quadratic non-linearity in (2.1) epitomises a number of natural phenomena in continuum. Its analytical properties have been exploited and elucidated for prototype problems in turbulence, shock formation and aerodynamics (see, for instance, Burgers 1974; Whitham 1974). Roughly speaking, the non-linear advection-diffusion term has an identical form as those in the Navier-Stokes equations; it represents the energy transport per unit mass on macroscopic scale:

$$u\partial_x u = \partial_x \left( \frac{1}{2} u^2 \right).$$

Then the energy integral

$$\int_0^1 u\partial_x u dx = \frac{1}{2} u^2 \Big|_0^1 = 0 \quad (2.5)$$

in view of the boundary conditions. The flux is determined by the normal gradients on the boundary

$$\frac{d}{dt} \int_0^1 u(x, t) dx = -\nu \frac{\partial u}{\partial x} \Big|_0, \quad (2.6)$$

that is conserved only in flows satisfying  $\partial_x u(0, t) = \partial_x u(1, t)$  (sometimes known as the second boundary value problems). The shear stress on the ‘wall’  $x = 1$  per unit density for (2.3) is given by

$$\tau_w = \nu \frac{\partial u}{\partial x} \Big|_w. \quad (2.7)$$

Similarly, we are interested in the local shear at the ‘centre’ of (2.4)  $\partial u/\partial x|_{x=0.5}$ .

Multiplying (2.1) by  $u$  and integrating the result over space, we obtain the energy conservation law

$$\frac{1}{2} \int_0^1 u^2 dx + \nu \int_0^t \left( \int_0^1 \left( \frac{\partial u}{\partial x} \right)^2 dx \right) dt = \frac{1}{2} \int_0^1 u_0^2 dx. \quad (2.8)$$

In addition, the energy law (2.8) shows that the velocity at any instant must satisfy

$$|u(x, t)| \leq A_0, \quad 0 < x < 1, \quad t > 0. \quad (2.9)$$

This bound may serve as a useful criterion to monitor computations. For convenience, we shall call the quantity  $\partial_x u / \partial x$  vorticity as it appears in the enstrophy relation in (2.8) even though it may be a strain on face value.

Green's function for the heat operator in (2.1) satisfying boundary conditions (2.2) is given by (for  $t > 0$ )

$$\begin{aligned} G(x, y, t) &= 2 \sum_{k=1}^{\infty} \sin(k\pi x) \sin(k\pi y) \exp(-\pi^2 k^2 \nu t) \\ &= \frac{1}{\sqrt{4\pi\nu t}} \sum_{k=-\infty}^{\infty} \left[ \exp\left(-\frac{(x-y-2k)^2}{4\nu t}\right) - \exp\left(-\frac{(x+y-2k)^2}{4\nu t}\right) \right]. \end{aligned} \quad (2.10)$$

By the summability of non-linearity (2.5), we are justified to make use of Duhamel's principle. Burgers' equation then satisfies the following integral equation

$$u(x, t) = w_0(x, t) + \int_0^t \int_0^1 K(x, y, t-s) u^2(y, s) dy ds, \quad (2.11)$$

where

$$w_0(x, t) = \int_0^1 G(x, y, t) u_0(y) dy,$$

and the kernel function  $K = \partial G / \partial y / 2$ . As shown in §8 and §12 of Lam (2013), the solution of (2.11) can be expressed in terms of a convergent series

$$\begin{aligned} u(x, t) &= \gamma^*(x, t) + 2 V[\gamma^*]^2 + 10 V[\gamma^*]^3 + 62 V[\gamma^*]^4 + 430 V[\gamma^*]^5 + 3194 V[\gamma^*]^6 \\ &\quad + 24850 V[\gamma^*]^7 + 199910 V[\gamma^*]^8 + 1649350 V[\gamma^*]^9 + \dots, \end{aligned} \quad (2.12)$$

where  $\gamma^*(x, t)$  satisfies the linear Volterra-Fredholm integral equation

$$\gamma^*(x, t) = w_0(x, t) + \int_0^t \int_0^1 K(x, y, t-s) \gamma^*(y, s) dy ds.$$

As a motion initiated from given finite data marches in time, more and more terms must be retained to represent the flow field. At every time  $t > 0$ , an increasing amount of vorticity of smaller scales must be generated by the non-linearity ( $u \partial_x u$ ) in order for the law of energy conservation to be fulfilled, thus producing enhanced

local shear thanks to the presence of viscosity. Effectively, the flow evolves into a collection of vortices of various length and time scales. Every scale,  $V[\gamma^*]^k$ , has a precise meaning and is defined by its space-time convolution of the initial data. This non-linear process of activating scales in abundance to balance instantaneous enstrophy production is described as *vorticity or scale proliferation*.

Evidently, it is a challenge to numerically evaluate all the terms of the series. In practice, one would prefer to bypass the direct evaluations but to solve the dynamic equation (2.1) by more efficient algorithms. Recall that one will certainly avoid tedious calculations of the Fredholm analytic expression for integral equations at face value; it is definitely beneficial to solve the governing differential equation by straight-forward numerical techniques.

The initial velocity (2.3) or (2.4) will evolve into space in time as  $u = u(x, t)$ . There does not exist a ‘steady’ velocity throughout the motion by virtue of (2.8) and (2.9). Lack of a characteristic velocity suggests that the flow development for  $t > 0$  cannot be expounded on dynamic similarity. On the basis of rigour, we do not identify viscosity as Reynolds number  $Re = 1/\nu$  in the initial-boundary problem. This view asserts that any time-independent flow generated in laboratory or in nature, if exists, must be preceded by a time-dependent dynamics which galvanises contiguous shear diversity.

### 3. Exact solutions at moderate viscosity

General solutions of Burgers’ equation can be written in a closed analytical form (Cole 1951; Hopf 1950). Equation (2.1) may be expressed in a conservative law

$$\frac{\partial u}{\partial t} = \frac{\partial}{\partial x} \left( \nu \partial_x u - \frac{1}{2} u^2 \right). \quad (3.1)$$

This formula suggests there exists a ‘similarity function’  $\psi(x, t)$  so that

$$u(x, t) = a \partial_x \psi(x, t)$$

for some constant  $a$ . A time differentiation shows the function is compatible to (3.1) or

$$(\partial_t - \nu \partial_{xx}) \psi = a (\partial_x \psi)^2 / 2. \quad (3.2)$$

In order to eliminate the non-linear right-hand, we introduce  $\psi = -b \log \phi(x, t)$ . By differentiation, we can express  $u$  in terms of  $\phi$ . Thus equation (3.1) is reduced to

$$-b \frac{\partial_t \phi}{\phi} = \nu b \left( \frac{\partial_x \phi}{\phi} \right)^2 - \nu b \frac{\partial_{xx} \phi}{\phi} - \frac{ab^2}{2} \left( \frac{\partial_x \phi}{\phi} \right)^2,$$

where it is clear that the non-linearity can be nullified if  $ab = 2\nu$ , leading to a linear heat equation

$$\partial_t \phi - \nu \partial_{xx} \phi = 0. \quad (3.3)$$

In particular, we obtain the Cole-Hopf transformation for  $a = 1$  and  $b = 2\nu$

$$u = a \partial_x \psi = -2\nu \frac{\partial_x \phi}{\phi}. \quad (3.4)$$

	$\nu = 10^{-3}$	$\nu = 10^{-4}$
$t = 0.25$	13.9337	14.5616
0.5	491.9831	4995.0574
1	269.9739	2710.8183
5	17.4706	176.4549
10	4.5980	46.8603
100	0.0397	0.4869
1000	0	0.0040

Table 1. Evaluation of analytic solution (3.4)-(3.6) by the scaling technique. Initial data  $u_0(x) = \sin(\pi x)$ . Results of  $-\partial_x u|_{x=1}$  or  $|\partial_x u|_w$  at selected time.

The initial condition for (3.3) can be obtained from (3.4)

$$\phi_0(x) = \phi(x, t = 0) = \exp\left(-\frac{1}{2\nu} \int_0^x u_0(y) dy\right). \quad (3.5)$$

Solutions  $\phi$  (and its derivatives) are found by convolution of Green's function and the initial data:

$$\phi(x, t) = \int_0^1 G(x, y, t) \phi_0(y) dy. \quad (3.6)$$

It is evident that (2.1) is regular for  $t > 0$  and categorically rules out blow-up in *real* fluids ( $\nu > 0$ ) having bounded initial energy.

#### Computation of exact solution

The transformed initial condition (3.5) can be evaluated without difficulty for  $\nu > 0.01$  by means of machine-aided computations as the Fourier series defining Green's function converges reasonably fast. As the viscosity becomes smaller, it is impractical to compute the analytic expression to acceptable accuracy because the exponential function in  $\phi_0$  would cause underflow or overflow as soon as we integrate away from  $x = 0$ , even over short time intervals. Since velocity  $u$  is given by a *ratio* of two rapid-changing exponentials, one remedy is that we scale both  $\phi$  and  $\phi_x$  by suitably chosen functions so that the numerical difficulty may be avoided. For instance, we can compute

$$\tilde{\phi}_0(x) = \exp(Q) \phi_0(x) \quad (3.7)$$

and then

$$\tilde{\phi}(x, t) = \int_0^1 G(x-y, t) \exp(P) \tilde{\phi}_0(y) dy, \quad (3.8)$$

where  $Q = Q(x, t, \nu)$  and  $P = P(x-y, t, \nu)$  are the scaling. In practice, it is tedious find a 'correct' pair as we must rely on trial and error. Nevertheless, it is clear that the pair are not unique and depend on the initial data as well as the local flow. The objective of evaluating the exact solutions in this manner is to verify a general-purpose numerical scheme developed in the present paper. In table 1, we list some results for viscosity down to  $10^{-4}$ . At least an order of magnitude improvement has been achieved compared to the best known exact solutions (Cole 1951; Basdevant, *et al.* 1986; Zhang *et al.* 1997).

#### 4. Numerical scheme for small viscosity $\nu$

We do not need to emphasise the importance of the simplest non-linear differential equation (2.1) as a prototype for the physics of fluid dynamics. Yet there does not seem to exist a reliable computational method at small viscosity  $\nu \lesssim 10^{-5}$ . Zhang *et al.* (1997) give a short review on standard numerical schemes such as finite difference and spectral technique. Unfortunately, none of these numerical methods appears to be capable of handling Burgers' equation in small-viscosity applications; detailed numerical data are scarce in literature. In a nutshell, the difficulty with these methods is their inability to resolve the finest spatio-temporal scales over the transitional regime. Specifically, among a number of published work in high Reynolds flow, there are significantly different solution behaviours over  $t = 0.2$  and  $t = 0.4$  at  $Re = 10^5$  for initial data (2.3). An alternative approach is the meshfree method of smoothed particle hydrodynamics. By an enhanced formulation, Hashemian & Shodja (2008) managed to calculate the velocity solutions at specific sets of particle distribution and variable dilation.

Surprisingly, the dynamics defined by (2.1) at small finite viscosity *is unknown* though efforts made on the theoretical inviscid limit ( $\nu = 0$ ) are well-documented. However, it is not the velocity but the vorticity field which enshrines the proliferation process. To explore the shear regime, we develop a numerical scheme which takes the advantage of variable mesh distribution and totality of spatio-temporal scales. The first feature allows improved discretisation in shear-intensity regions for high efficiency while the second is crucial in complete capture of (continuum) turbulence. The trapezoidal rule is used to approximate kernel convolution in conjunction with an implicit Euler method for time marching. As the convolution carries over smooth functions, intermediate mesh grids can be obtained by any suitable interpolation procedure as long as the solutions remain differentiable (analogous to ideas in Adams-Bashforth methods). To be definite, the grid for case  $u_0(x) = \sin(\pi x)$  is distributed according to formula

$$x_i = \frac{1}{2} + \frac{\tanh(\sigma(2i-n-1)/(n-1))}{2 \tanh \sigma}, \quad (4.1)$$

where the stretching parameter  $\sigma$  is used to control the grid spacings near both ends at given grid point  $n$ . Similar ideas are applied to the shear flow (2.4), formula,

$$x_i = \frac{\tanh(2\sigma(i-1)/(n-1))}{2 \tanh \sigma}, \quad (4.2)$$

generates grids in one half of the domain so as to cluster more points near the centre  $x = 0.5$ . (Either can be enhanced in self-adaptive schemes for calculations of complicated moving shear field.) The approximation error is proportional to  $(\Delta t)(\Delta x)^2$ . It is found that the time step  $\Delta t$  has to be one or two order of magnitude *lower* than viscosity  $\nu$  in order to maintain numerical stability over the phase of non-linear growth. In the initial and decay phases, larger time steps (one or two order higher than  $\nu$ ) may be chosen to cut down numbers of iteration. It is a practical matter of trade-off between time  $\Delta t$  and iterations. The majority of our calculations reach a prescribed convergence tolerance ( $10^{-14}$ ) on a Euclidean norm of velocity  $u$  in less than 10 iterations at specified time step. A typical calculation, say from  $t = 0$  to  $t = 1$  for  $\nu \sim O(10^{-6})$ , requires  $O(10^7)$  time steps to complete. The storage

	$\sigma / n$ in (4.1)	$\Delta t$	$ \partial_x u _{\max}$	$t$ for $ \partial_x u _{\max}$
Exact			495.028422	0.503023
Numerical	4.0 / 121	$1 \times 10^{-4}$	495.35	0.50320
	4.0 / 121	$1 \times 10^{-5}$	495.93	0.50302
	4.0 / 161	$1 \times 10^{-4}$	495.24	0.50320
	4.0 / 161	$5 \times 10^{-5}$	495.11	0.50310
	4.0 / 161	$1 \times 10^{-5}$	495.40	0.50303
	4.0 / 201	$1 \times 10^{-4}$	495.21	0.50320
	5.0 / 201	$1 \times 10^{-4}$	495.24	0.50320
	3.0 / 201	$1 \times 10^{-4}$	495.21	0.50320

Table 2. Effect of numerical parameters on solution accuracy. Viscosity  $\nu = 1 \times 10^{-3}$ ,  $u_0(x) = \sin(\pi x)$  with homogeneous boundary condition at  $x = 0$  and  $x = 1$ . The maximum derivative is found to occur at wall  $x=1$ .

requirement is roughly  $O(n^2)$  and hence is almost negligible in view of modern computer power. Our numerical scheme demonstrates that accurate solutions of Burgers' equation down to viscosity one billionth ( $\nu = 10^{-9}$ ) can be obtained on a 64-bit desktop machine with a quad-core microprocessor.

#### Wall shear layer

Validations of our numerical method are first made with exact solution (3.4)-(3.6) computed according to scheme (3.7)-(3.8) (see table 2). As a matter of fact, over 99% of Burgers' flow evolves significantly in an ultra-thin width at the wall  $\sim O(0.005)$  and hence 90% computational effort is allocated to the flow in the vicinity of  $x \approx 1$ . It is over this dissipative region that the flow possesses scales of various sizes and nearly consumes all the initial kinetic energy. Even at viscosity  $\nu = 10^{-3}$ , the wall vorticity is increased 160 times in a time interval of 0.5!

One crucial aspect in computational fluid dynamics is how to resolve the broad range of scales in high Reynolds number flow. As the Navier-Stokes equations are globally regular, all of the scales in turbulence must be taken into account on the basis of the continuum (Bradshaw 1971; Tennekes & Lumley 1972; Davidson 2004). Solutions of Burgers' equation represent the (ensemble) mean values at space-time location  $(x, t)$  for every given finite viscosity. Practically, machine-aided computations are limited by finite precision arithmetic. In real turbulence, there exists a natural cut-off on the flow scales as viscous dissipation cannot be an instantaneous process and must proceed on finite spatial scales.<sup>†</sup> The results given in tables 3 and 4 show that the spatial resolution in our computations is adequate though somehow over-killed. By performing additional numerical experiments, we establish a simple rule of thumb: *the minimum cut-off scale has to be at least two orders of magnitude smaller than viscosity.*

<sup>†</sup> The K41 hypotheses on turbulence (Kolmogorov 1941a, 1941b) do not apply to our computations as, evidently, the evolved flow field from initial data (2.3) or (2.4) cannot be regarded as homogeneous and 'isotropic'. Nevertheless, it is interesting to notice that the Kolmogorov dissipation scale for fully-developed turbulence should be  $\eta \sim O(\nu^{4/3})$ , taking the integral scale  $l_0$  as unity. Thus the mean dissipation rate  $\varepsilon \sim u^3/l_0 \sim O(1)$  in the present models.



Cut-off	$10^{-5}$	$10^{-6}$	$10^{-7}$	$\epsilon$
$t = 0.3$	37.402	52.130	54.019	54.220
0.32	$1.357 \times 10^2$	$9.602 \times 10^2$	$1.318 \times 10^3$	$1.361 \times 10^3$
0.34	$8.756 \times 10^3$	$1.625 \times 10^4$	$1.700 \times 10^4$	$1.709 \times 10^4$
0.4	$2.898 \times 10^4$	$4.022 \times 10^4$	$4.139 \times 10^4$	$4.146 \times 10^4$

Table 3. Result of  $-\partial_x u|_w$  over ‘transition’ regime. Viscosity  $\nu = 10^{-5}$ ,  $u_0(x) = \sin(\pi x)$ . For all the runs,  $n = 181$  and time marching  $\Delta t = 10^{-5}$ , and  $2 \times 10^{-6}$ . The symbol  $\epsilon \approx 2 \times 10^{-19}$  denotes the cut-off scale used in the present work. Roughly, it equals to a specific floating-point precision implemented by GNU FORTRAN 95 compiler.

Cut-off	$10^{-6}$	$10^{-7}$	$10^{-8}$	$\epsilon$
$t = 0.2$	4.572	4.580	4.581	4.581
0.3	52.518	54.634	54.632	54.652
0.32	$7.112 \times 10^3$	$1.517 \times 10^4$	$1.523 \times 10^4$	$1.530 \times 10^4$
0.34	$1.592 \times 10^5$	$1.704 \times 10^5$	$1.714 \times 10^5$	$1.713 \times 10^5$
0.4	$3.686 \times 10^5$	$4.099 \times 10^5$	$4.149 \times 10^5$	$4.147 \times 10^5$
0.5	$3.900 \times 10^5$	$4.892 \times 10^5$	$5.007 \times 10^5$	$5.006 \times 10^5$
0.6	$3.241 \times 10^5$	$4.533 \times 10^5$	$4.685 \times 10^5$	$4.691 \times 10^5$

Table 4. See table 3,  $\nu = 10^{-6}$  and the shortest  $\Delta t = 2 \times 10^{-7}$ . The flow remains ‘laminar’ during the initial phase  $0 \leq t < 0.319$ . Scale proliferation starts at  $t \approx 0.319$ . At  $t \approx 0.5$  and onward, the flow in the wall vicinity evolves into the ‘fully-developed turbulent’ state.

### Free shear flow

As we have entered the arena of computations at extremely small viscosity, some efforts have been made to nurse the present low- $\nu$  calculations, particularly on the suitable choice of time steps  $\Delta t$ . Should  $\Delta t$  be too coarse, there are problems of convergence; too fine, of accumulations of excessive round-off errors. The diverging scenario is easy to diagnose during computations while the latter difficulty is rather tricky to quantify. We are well aware of the fact that it is impossible for machine-aided computations to immune from round-off.

The velocity bound (2.9) serves as an indication as the integrations are undertaken from  $x = 0$  to  $x = 1$ . Reversal of the integrations from  $x = 1$  to  $x = 0$  may provide useful hints on the degrees of round-off. Another reason to examine shear flow (2.4) is its symmetry. As our calculations proceed, we monitor the development of one-direction sums, for instance, the integrated velocity profiles in  $0 < x < 0.5$  and  $0.5 < x < 1$  over  $10^7$  time steps. Significant departure from velocity symmetry gives us some ideas about the seriousness of accumulating errors. These methods are entirely empirical and are found to work well for the viscosity range studied in the present paper.

We find that reliable flow solutions for  $\nu > 10^{-6}$  can be easily computed in double precision arithmetic. As a practical guide, use of higher precision floating point representation in programming language (for instance, the variable type `real(kind=16)` in modern FORTRAN) is probably one of the most effective ways to minimise the round-off errors, assuming the computations may be performed in reasonably manageable time. It is anticipated that accurate solutions of Burgers’ equation for any given viscosity value are achievable by the present algorithm on more powerful machines. In practice, a Reynolds number in the order of one trillion

$x$	$u$ (Exact)	$u$ (Num.)	$u$ (H-S 2008)	$\partial_x u$ (Exact)	$\partial_x u$ (Num.)
0.05	0.03792	0.03792	0.0379	0.75837	0.75838
0.11	0.08341	0.08341	0.0834	0.75786	0.75787
0.16	0.12129	0.12129	0.1213	0.75714	0.75715
0.22	0.16668	0.16668	0.1667	0.75591	0.75592
0.27	0.20444	0.20445	0.2044	0.75457	0.75457
0.33	0.24966	0.24966	0.2497	0.75255	0.75256
0.38	0.28724	0.28724	0.2872	0.75052	0.75053
0.44	0.33219	0.33219	0.3322	0.74762	0.74763
0.50	0.37694	0.37695	0.3769	0.74417	0.74418
0.55	0.41407	0.41407	0.4141	0.74084	0.74085
0.61	0.45839	0.45839	0.4584	0.73622	0.73622
0.66	0.49509	0.49509	0.4951	0.73179	0.73179
0.72	0.53882	0.53882	0.5388	0.72568	0.72568
0.77	0.57496	0.57496	0.5749	0.71982	0.71982
0.83	0.61791	0.61791	0.6179	0.71170	0.71170
0.88	0.65330	0.65331	0.6533	0.70388	0.70387
0.94	0.69522	0.69522	0.6952	0.69291	0.69291
0.96	0.70903	0.70904	0.7090	0.68882	0.68881
0.98	0.72277	0.72277	0.7228	0.68446	0.68446
0.99	0.72960	0.72960	0.7296	0.68219	0.68218
0.995	0.73301	0.73301	0.7330	0.68102	0.68101
0.999	0.73480	0.73482	0.7348	-6.18320	-6.18259*
0.9995	0.69991	0.69998	0.6999	-259.09	-259.05
0.9999	0.25946	0.25955	0.2599	-2374.05	-2374.45
1.0	0	$O(10^{-20})$	-	-2710.82	-2712.01

Table 5. Solutions of Burgers' equation at  $t=1$  for  $A_0=1$  in initial profile (2.3),  $\nu=10^{-4}$ . The exact values are obtained by the proposed procedure (3.7)-(3.8). The present numerical calculations (Num.) are carried out with grid points  $n = 161, 181, 201, 221, 241, 261$ , and  $\sigma = 5$  at time steps  $\Delta t = 1 \times 10^{-5}$  and  $5 \times 10^{-6}$ . Over the region  $0.99 \lesssim x \leq 1$ , we have collocated 45, 50, 55, 60, 65, 70 grid points respectively. The results of our computations are found to be independent of the grids. The noticeable discrepancy is only in the last three  $x$  locations; these data agree within a relative band of  $\pm 0.02\%$ . Our data are the values at  $n = 201$ . (\*This value is the only exception; it is extrapolated from the runs.) In particular, the wall shear  $-\nu \partial_x u|_w$  is found to be  $0.2712 \pm 0.0003$ .

$O(10^{12})$  is likely over-specified for the great majority of earth-bound incompressible flows.

## 5. Flow developing stages

### (a) Rapid shear build-up

In table 5, we compare our numerical solutions with exact values for the case of  $\nu = 10^{-4}$ . Also included are the results of Hashemian & Shodja (2008). In figures 1 and 2, we display our computational results for  $\nu = 10^{-5}$ . The effect of viscosity is examined in figures 3 and 4. Detailed local vorticity intensifications are given in figures 5-6. The snapshots on the right columns show that the shears over the vorticity growth approach to the wall with zero gradient - a property established in

$t$	$-\partial_x u _w$
223	1
703	$10^{-1}$
2190	$10^{-2}$
6597	$10^{-3}$
17925	$10^{-4}$
37745	$10^{-5}$
60605	$10^{-6}$

Table 6. Decay of wall shear as time  $t \rightarrow \infty$ . Data  $u_0(x) = \sin(\pi x)$  and  $\nu = 10^{-5}$ . The large time stated on the left below the third row is for indicative purposes. As a rough guide, the maximum velocity drops below  $10^{-5}$  after  $t > 10^5$ .

experiment on turbulent shear stress (see §Turbulence intensity and shearing stress in Klebanoff 1955). The rapid accumulation of vorticity is not restricted to wall region. Figure 7 demonstrates the formation of shock waves, which are intensified viscous shears having finite thickness. The size of initial data determines the initial moment of the abrupt vorticity build-up (figures 8-9).

(b) *Overshoot in local enstrophy*

We have mentioned that the vorticity intensification is a direct consequence of the non-linearity in the equation. Our solutions show that the development enstrophy in Burgers' equation actually reaches a maximum, depending on the strength of the initial data. The phenomenon of 'overshoot' in local skin friction was firstly established in boundary layer experiments, see, for example, Coles (1954). In figures 10 and 11, we present selected computations which verify the existence of the overshoot in our continuum fluid model. The results are given in terms of the local enstrophy as it is a quantity applicable to shear layers as well. For the sake of reference, we plot the local 'skin friction' coefficient in figure 12.

In terms of the intermittency distribution of turbulent spots collected from experiments, Narasimha (1984) gave an empirical explanation of the skin-friction overshoot. In the framework of boundary layer approximations, the overshoot was further explained and was attributed to an origin shift of the developing turbulent boundary layer over the transition zone (p. 385 of Narasimha 2011). For some practical purposes, the fitted theory may be adequate. The overshoot phenomenon, which was often discounted (p. 639 of Schlichting 1979), is in fact an evolution phase in any fluid motion undergoing the laminar-turbulent transition, particularly the natural one. If we are dealing with the full equations of motion, the concept of a boundary layer becomes somehow blurred. The present computational results reveal that *the overshoot in the local enstrophy is a characteristic of the non-linear vorticity build-up over the transition period.*

(c) *Long time decay*

The energy conservation suggests that strong dissipation exists over the thin viscous layer over a long period of time, and thus the velocity undergoes sustained decay. Table 6 shows the decay of the wall vorticity. Figure 13 shows that the turbulence quickly 'forgets' its initial energy content at small viscosity. The characteristic

of the long-time decay is presented in figure 14. For  $\nu < 10^{-5}$  ( $A_0 = 1$ ), the local enstrophy attenuates according to

$$\partial u / \partial x|_w \sim t^{-2.05} \quad \text{as} \quad t \rightarrow \infty$$

in the boundary layer starting from (2.3), and

$$\partial u / \partial x|_c \sim t^{-2} \quad \text{as} \quad t \rightarrow \infty$$

at the location of the maximum viscous dissipation in the turbulent free-shear originated from data (2.4). The decay graphs in figure 13 assert that the initial data (known as large eddies) have no influence on the attenuation rate. Hence these decay laws are valid for arbitrary finite  $A_0$ .

Since the vorticity near the wall or around the centre accounts for over 95% of the total shear strength, the local decays suggest that the law of energy decay is

$$\int_0^1 u^2(x, t) dx \sim t^{-1} \quad \text{as} \quad t \rightarrow \infty.$$

## 6. Experiments in flow transition

Out numerical results may be compared to experiment, particularly to the case of Blasius boundary layer on a flat plate. To relate the calculations to experiments, we may take the length scale  $x = 1$  m and the initial speed  $|u_0| = 1$  m/s. The phenomenon of the shear intensification takes place in a time  $t \sim O(10^{-3})$  s in fluids with viscosity  $\nu = 10^{-5}$  m<sup>2</sup>/s.

It is established in laboratory experiment that there is an abrupt growth in wall shear over transition region, see, for example, Schubauer & Klebanoff (1955). At a free stream turbulence level of 0.03%, the observed laminar-turbulent transition cannot be distorted by the free-stream turbulence intensity; the test transition is therefore the intrinsic transition embedded in the Navier-Stokes equations. From figure 3 of Schubauer & Klebanoff, the shear increase occurs over a time interval of  $3 \times 10^{-3}$  s, given a uniform free-stream speed of 24.38 m/s. Moreover, referring to their figure 4, the intense vorticity concentrates in a spatial length scale of 1.5 mm. Comparing the measurements (figure 15) and the numerical simulation (figure 16), the measured abrupt increase in wall shear is in qualitative agreement. The scale proliferation anticipates the time-wise occurrence of the shear build-up (the laminar-turbulent transition). The familiar friction jump over the transition (figure 17) is a consequence of the non-linear growth.

## 7. Discussion

Even though Burgers' equation is merely one-dimensional, its solutions provide convincing evidence on the process of the scale proliferation which is essentially responsible for the abrupt local vorticity intensification.

Turbulence is characterised by vortices of multitudinous scales whose topology encompasses a variety of geometry subject to continuous modifications by momentum transfer and diffusion. To describe turbulence in terms of Fourier components

requires justification because the flow scales defined by means of the wave components are certainly misguided portrayals of the genuine spatio-temporal structure. A critical précis on this fundamental issue is given in §6.6.4 of Davidson (2004).

On the continuum, the propensity for free deformation characterises fluids and is a precursor to resist instability. Analytically, motions of both laminar and turbulent states are governed by the Navier-Stokes equations, *not* by Ginzburg-Landau or Kuramoto-Sivashinsky equation. Solutions of the full equations are globally regular and hence they do not bifurcate in space and in time. Specifically, the solutions cannot develop any finite-time singularity for any initial data of bounded energy. It has been established in careful experiments that the laminar-turbulent transition *persists* once the free-stream turbulence or the acoustic noise are below some threshold level (Schubauer & Skramstad 1947; Wells 1967). The intensive local accumulation of vorticity is not connected to absolute instability engendered by spatially-amplified disturbances at selective frequencies; the apparent flow breakdown at fixed spatial locations observed in experiments is nothing more than a misreading of the fine-scale dynamic evolution.

Although the intrinsic transition is fully instigated by the non-linearity, disturbances may be abundant in varied forms in practice. Frequently, an observed transition is an aberration of the non-linear process. However, the disturbances can be quantified and specified as part of the initial or boundary conditions; the modified problem is well-defined and hence computationally tractable.†

In application, we may consider the effect of external control by adding a prescribed force,  $f(x, t)$ , to Burgers' equation. Similarly, the no-slip boundary conditions may be suitably modified in design of flow control. Since the equation resembles the vorticity equation for 2-dimensional incompressible viscous flow, investigation of the vorticity evolution at high Reynolds numbers looks promising. In fact, our numerical scheme needs minor modifications so as to embrace vorticity stretching  $(\omega \cdot \nabla)u$  in 3 space dimensions. As expected, the computation cost will be more substantial but would no longer be prohibitively expensive. The non-local nature of vorticity on velocity has to be taken into account and its effect is expected to reduce overall shear strength.

## 8. Conclusion

Burgers' equation is innocuous but is a well-chosen model for the full Navier-Stokes equations as they share many of the essential analytic characters. From the present study, we are able to advance our understanding in one critical aspect: the governing equations furnish a reliable tool for predicting the laminar-turbulent transition, not

† Our view contradicts those of instability theory, which claims success in a few incompressible cases. Taylor's paper on Couette flow between co-axial rotating cylinders (Taylor 1923) is not an instability analysis but the *bona fide* method of eigen-function expansion applied to the linearised equations. The 'disturbances' consist of non-amplifying Fourier components. There are no particular reasons to suspect its success over the initial phase of flow development in that specific topology. In the flat-plate experiment of Schubauer & Skramstad (1947), artificial disturbances of known frequencies were intentionally introduced. The rationale for the good comparison with linear stability theory is that the Blasius mean flow is a credible *non-linear solution* in view of the boundary layer approximations (Prandtl 1904). Thus the infinitesimally perturbed laminar layer remains well-estimated by linearisation over the low-Reynolds-number regime close to plate's leading edge where the hypothesised local similarity holds.

only for the onset of the phenomenon but the complete process. In an averaged sense, the transition is an intrinsic part of the flow evolution driven by the non-linearity and the energy conservation. In reality, viscous dissipation occurs at all time and stirs up randomness when the vorticity proliferation is amply operational. Turbulence is the incessant assembly of material subdivision. It is a fundamental fact that the transitional dynamics is Galilean invariant.

Real shock waves and viscous wall layers have finite thickness  $\sim O(\nu)$ . Viscosity is the key as it determines the spatial scales in the shear layers and irons out any discontinuity. We summarise the development of shear flows in several generic stages: (1) The initial shear growth is almost linearly with time at all values of viscosity; (2) There exists a time interval in which shear strength in localised region abruptly increases. The surge in vorticity due to the non-linearity marks the birth of turbulence; (3) The end stage is easily identified when the local enstrophy attains a maximum value; (4) The flow is fully turbulent and subsequently hibernates in a lengthy decaying period, particularly at small viscosity. The decay is governed by a power-law of time.

The mathematical form of equation (2.1) is identical to the KPZ equation (Kardar *et al.* 1986) for material interface growth or erosion due to vapour deposition. In astrophysics, suggestion has been put forward to use 3d Burgers' equation to model long-time self-organisation of the large structure in the Universe (see, for example, Woyczyński 1998). The model is expected to be able to simulate formation of cellular structures in mass distribution.

No claims have ever been made on the validity of the continuum hypothesis at all spatio-temporal scales. It is well-established, from physics, that diffusion equation and the equations of general relativity have their limitations at atomic scales or are surely invalid at the Planck scale of length and time. Ironically, the global regularity of equation (2.1) and of (1.1) asserts that these equations of fluid motion hold beyond the Planck scales for finite  $\nu > 0$ ! The essence is that Burgers' equation or its Navier-Stokes progenitor offers a trustworthy model for the understanding of numerous practical problems formulated within the paradigm of Newtonian mechanics and classical thermodynamics.

22 February 2016  
f.lam11@yahoo.com

## References

- Basdevant, C., Deville, M., Haldenwang, P., Lacroix, J.M., Ouazzani, J. Peyret, R., Orlandi, P. & Patera, A.T. 1986 Spectral and finite difference solutions of the Burgers equation. *Comput. Fluids*, **14**(1), 23-41.
- Bradshaw, P. 1971 *An Introduction to Turbulence and its Measurement*. Oxford: Pergamon Press.
- Burgers, J.M. 1948 A mathematical model illustrating the theory of turbulence. *Adv. Appl. Mech.*, **1**, 171-199.
- Burgers, J.M. 1974 *The Nonlinear Diffusion Equation. Asymptotic Solutions and Statistical Problems*. Dordrecht-Holland/Boston-U.S.A.: Reidel Publishing Company.
- Cole, J.D. 1951 On a quasi-linear parabolic equations occurring in aerodynamics. *Quart. Appl. Math.*, **9**, 225-236.

- Coles, D.E. 1954 Measurements of turbulent friction on a smooth flat plate in supersonic flow. *J. Aero. Sci.*, **21**, 433-448.
- Davidson, P.A. 2004 *Turbulence - An Introduction for Scientists and Engineers*. Oxford: Oxford University Press.
- Hashemian, A. & Shodja, H.M. 2008 A meshless approach for solution of Burgers' equation. *J. Comput. Appl. Math.*, **220**, 226-239.
- Hopf, E. 1950 The partial differential equation  $u_t + uu_x = \mu u_{xx}$ . *Comm. Pure Appl. Math.*, **3**, 201-230.
- Kardar, M., Parisi, G. & Zhang, Y.C. 1986 Dynamical scaling of growing interfaces. *Phys. Rev. Lett.*, **56**, 889-892.
- Klebanoff, P.S. 1955 Characteristics of turbulence in a boundary layer with zero pressure gradient. *Rep. Nat. Adv. Comm. Aero. Wash.*, **1247**.
- Kolmogorov, A.N. 1941a The local structure of turbulence in incompressible viscous fluid for very large Reynolds numbers. *Dokl. Akad. Nauk SSSR*, **30(4)**, 9-13. (Reprinted in *Proc. Roy. Soc.*, **A434**, 9-13 (1991).)
- Kolmogorov, A.N. 1941b Dissipation of energy in locally isotropic turbulence. *Dokl. Akad. Nauk SSSR*, **32(1)**, 16-18. (Reprinted in *Proc. Roy. Soc.*, **A434**, 15-17 (1991).)
- Lam, F. 2013 Integral invariance and non-linearity reduction for proliferating vorticity scales in fluid dynamics. [arXiv:1311.6395v4](https://arxiv.org/abs/1311.6395v4) [physics.flu-dyn].
- Lighthill, M.J. 1963 Introduction. Boundary Layer Theory. In *Laminar Boundary Layers* (ed. L. Rosenhead), pp. 46-113. New York: Dover.
- Narasimha, R. 1985 The laminar-turbulent transition zone in boundary layer. *Prog. Aero. Sci.*, **22**, 29-80.
- Narasimha, R. 2011 Satish Dhawan. In *A Voyage Through Turbulence* (ed. P.A. Davidson), pp. 373-391. Cambridge: Cambridge University Press.
- Prandtl, L. 1904 Über flüssigkeitsbewegungen bei sehr kleiner Reibung. *Verh. Int. Math. Kongr., Heidelberg*, pp. 484-494, Germany: Teubner, 1905. Also *Vier Abhandlungen zur Hydrodynamik und Aerodynamik* (1927), pp. 1-8, Göttingen. English translation: Motion of fluids with very little viscosity, *Tech. Memo. Nat. Adv. Comm. Aero. Wash.*, **452**.
- Reynolds, O. 1883 An experimental investigation of the circumstances which determine whether the motion of water shall be direct or sinuous, and of the law of resistance in parallel channels. *Phil. Trans. Roy. Soc.*, **174**, 935-982. Also *Scientific papers* (1901), vol. II, pp. 51-105. Cambridge University Press.
- Schlichting, H. 1979 *Boundary-Layer Theory*, 7th edn. New York: McGraw-Hill.
- Schubauer, G.B. & Klebanoff, P.S. 1955 Contributions on the mechanics of boundary-layer transition. *Rep. Nat. Adv. Comm. Aero. Wash.*, **1289**.
- Schubauer, G.B. & Skramstad, H.K. 1947 Laminar boundary-layer oscillations and transition on a flat plate. *J. Res. Nat. Bur. Stand.*, **38**, 251-292.
- Suder, K.L., O'Brien, J.E. & Reshotko, E. 1988 Experimental study of bypass transition in a boundary layer. *NASA Tech. Mem.*, **TM-100913**.
- Taylor, G.I. 1923 Stability of a viscous liquid contained between two rotating cylinders. *Phil. Trans. Roy. Soc.*, **A 223**, 289-343. Also *Scientific papers* (1971), vol. IV, pp. 34-85. Cambridge University Press.
- Tennekes, H. & Lumley, J.L. 1972 *A First Course in Turbulence*. Cambridge MA: MIT Press.
- Wells, C.S. 1967 Effect of free-stream turbulence on boundary-layer transition. *AIAA J.*, **5**, 172-174.
- Whitham, G.B. 1974 *Linear and Non-linear Waves*. New York: John Wiley & Sons.
- Woyczyński, W.A. 1998 *Burgers-KPZ Turbulence*. Berlin-Heidelberg: Springer-Verlag.
- Zhang, D.S., Wei, G.W., Kouri, D.J. & Hoffman, D.K. 1997 Burgers' equation with high Reynolds number. *Phys. Fluids*, **9(6)**, 1153-1155.

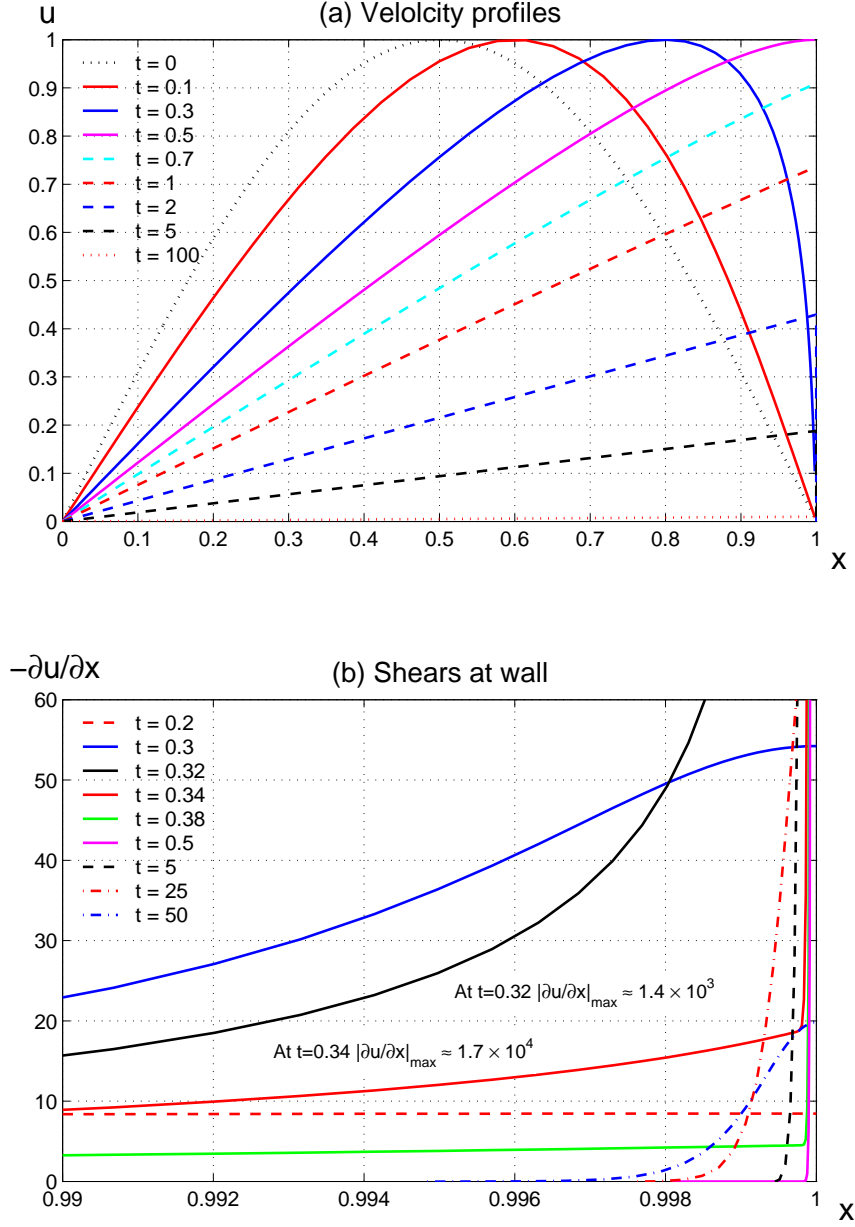


Figure 1. Initial velocity  $u_0(x) = \sin(\pi x)$ ,  $\nu = 10^{-5}$ . The calculation was done with a grid distribution of  $n = 181$  and  $\sigma = 7$  as defined in (4.1). To ensure fast convergence, the time marching was carried out at  $\Delta t = 10^{-5}$  to  $10^{-6}$ . The profile at  $t = 0.5$  is associated with the maximum shear ( $|\partial_x u|_w \approx 5 \times 10^4$ ). The overall development in velocity profiles (a) looks mundane. But vorticity evolves from initial value  $\pi \cos(\pi x)$  and coalesces into a thickness  $\sim O(\nu)$  next to the wall, as shown in (b). From  $t \approx 0.3$  onward, the growth in  $|\partial u / \partial x|$  proceeds in  $\Delta t \approx 0.05$  over a mere length  $\Delta x \approx 0.001$ ! The viscous wall layer has been well resolved; there are 45 grid points over  $0.99 \lesssim x \leq 1$ .



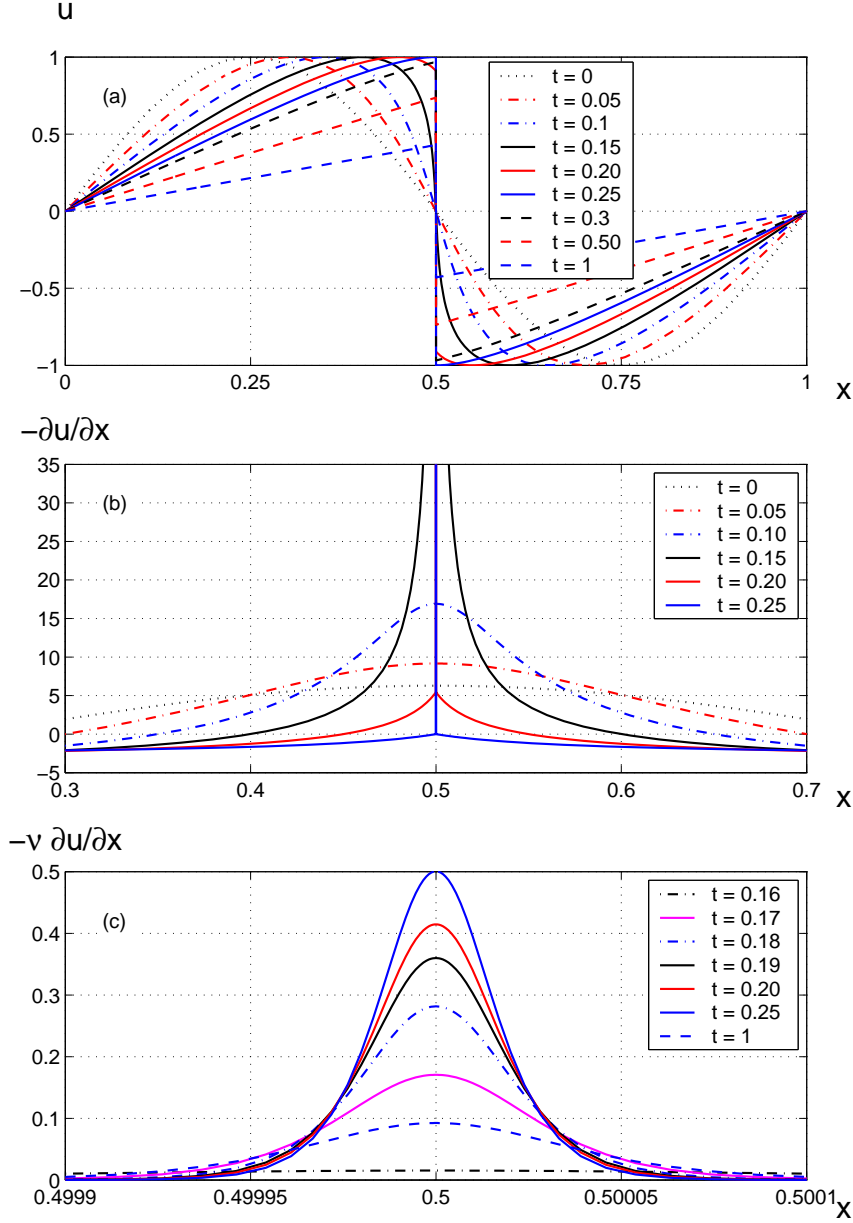


Figure 2. Abrupt coalesce of vorticity to form a ‘shock’ in the free-shear layer modelled by initial data  $u_0(x) = \sin(2\pi x)$  at  $\nu = 10^{-5}$ . Velocity profiles in (a) rapidly evolve into a cliff-edge topology in which a large amount of the initial energy clusters. The derivatives show the intensification of the shearing motion at the centre from  $t \approx 0.158$  to  $0.25$ , giving rise to an apparent singularity, see (b). The zoom-in of the coalesced region (c) however reveals the smoothness of the accumulated vorticity. The shock has a finite thickness in which viscous dissipation is intensive. The subsequent decay is somehow extremely slow in the thin layer due mainly to the small viscosity (cf. figure 1).

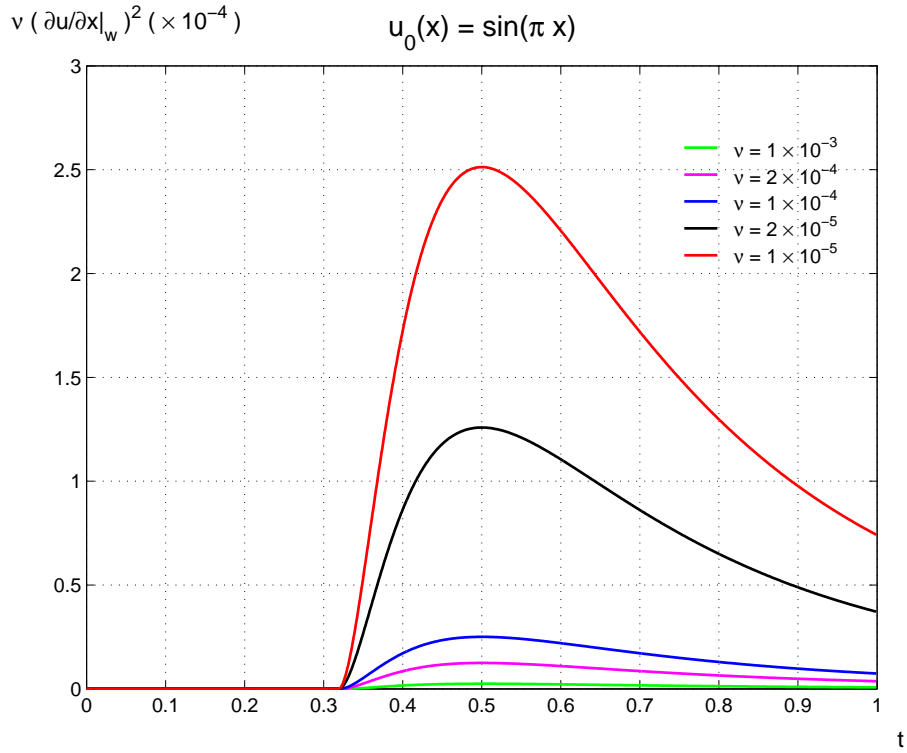


Figure 3. The vorticity growth is a consequence of the energy conservation. Evolution of wall enstrophy from the initial vorticity  $\partial_x u_0(x) = \pi \cos(\pi x)$  at several viscosity values. The initiation phase of the vorticity build-up depends weakly on viscosity. However, the rapid vorticity increase occurs readily in the flows of low viscosity (cf. typical high Reynolds-number flows).

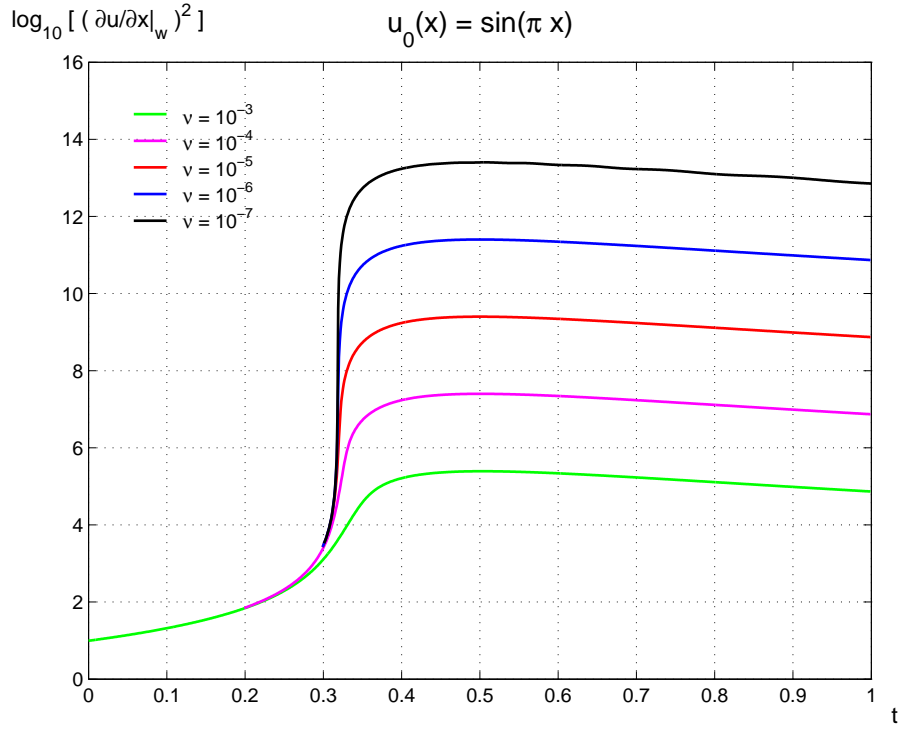


Figure 4. Evolution of wall entrophy as a function of viscosity. At instant  $t \approx 0.319$ , the wall entrophy or the vorticity starts to intensify. The build-up is a direct consequence of the scale proliferation by the non-linearity (2.12). There are much more vortices of smaller length scales in flows at low viscosity. Prior to the build-up  $0 < t < 0.319$ , the vorticity grows almost linearly: for example, at  $t = 0.3$ ,  $|\partial_x u|_w = 55.05, 54.65$  and  $54.22$  for viscosity  $10^{-7}, 10^{-6}$  and  $10^{-5}$  respectively.

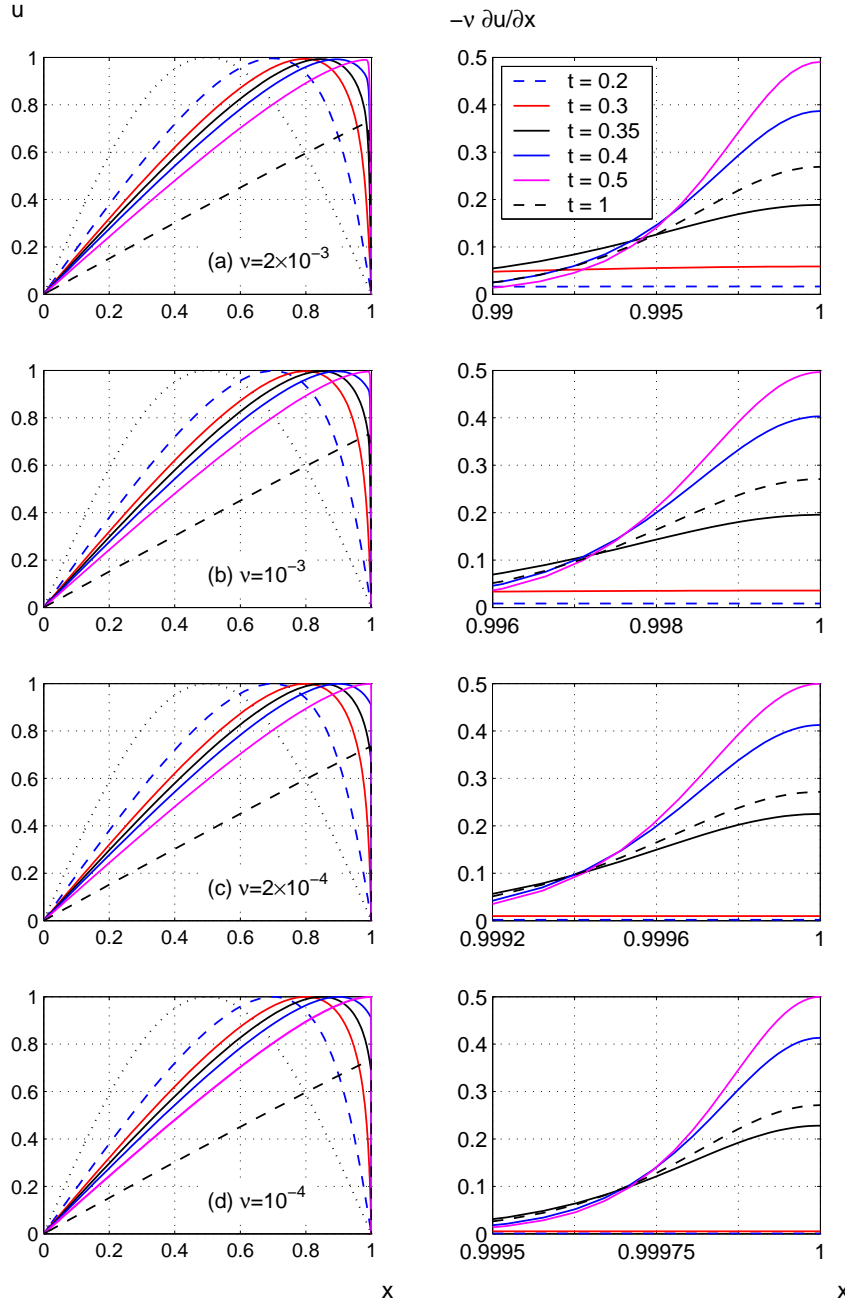


Figure 5. At large viscosity,  $\nu > 1 \times 10^{-3}$  for  $u_0(x) = \sin(\pi x)$ , the increase in shears from  $t = 0.3$  to  $t = 0.35$  is relatively weak. In (a) and (b), the profiles between  $0.3 \leq t \leq 0.5$  are not fully coalesced into the narrow wall region.

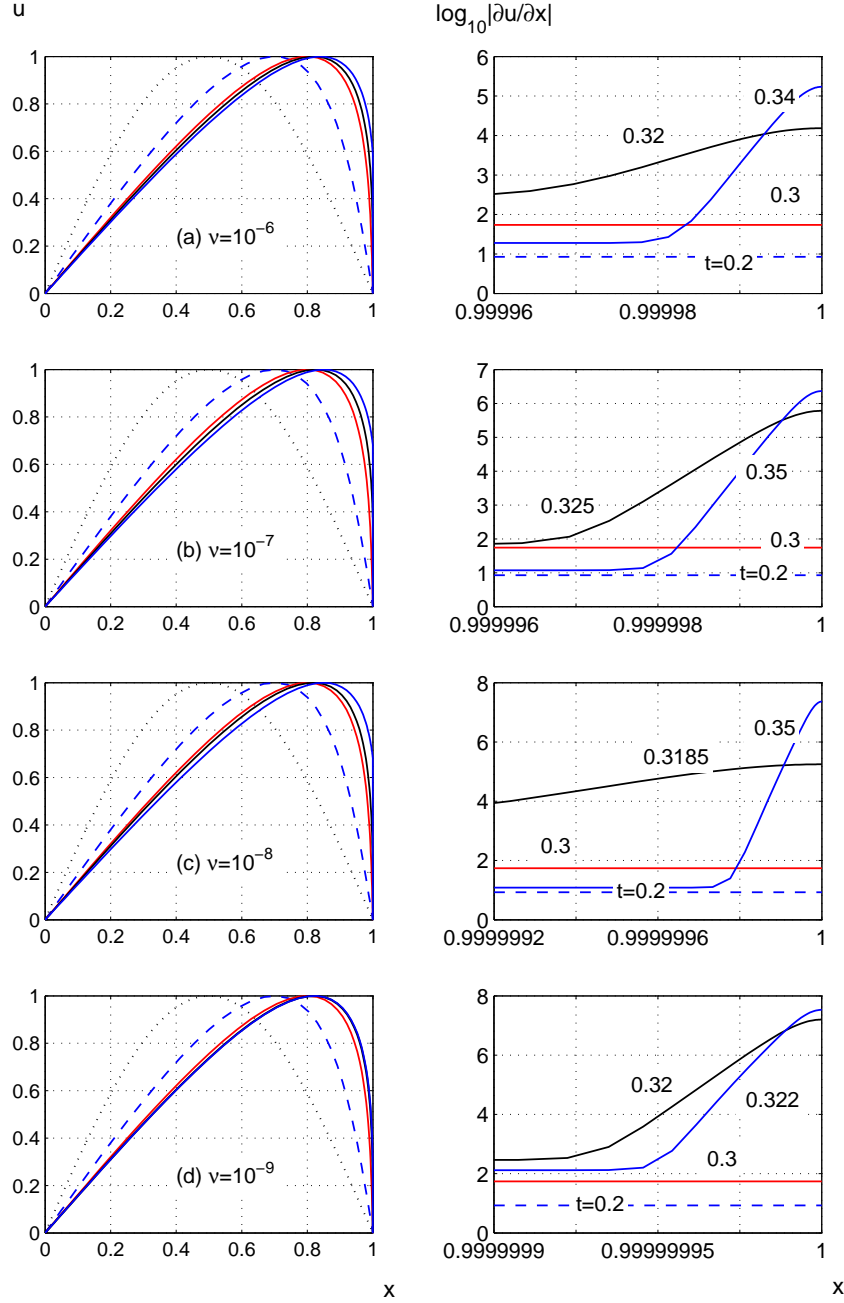


Figure 6. Effect of viscosity up to  $\nu = 10^{-9}$ . From top to bottom row, grid meshes  $(n, \sigma)$  are  $(201, 8)$ ,  $(211, 9)$ ,  $(231, 10)$  and  $(251, 11)$  respectively. The general trend of the shear build-up follows that of higher viscosity but the upsurges occur more rapidly. The wall vorticity is multiplied by several orders of magnitude in an interval  $\Delta t \sim O(0.005)$ . However, the modification in the velocity profiles seems insignificant. In terms of practical time and length scales, these flows are easily perceived as ‘broken down’.

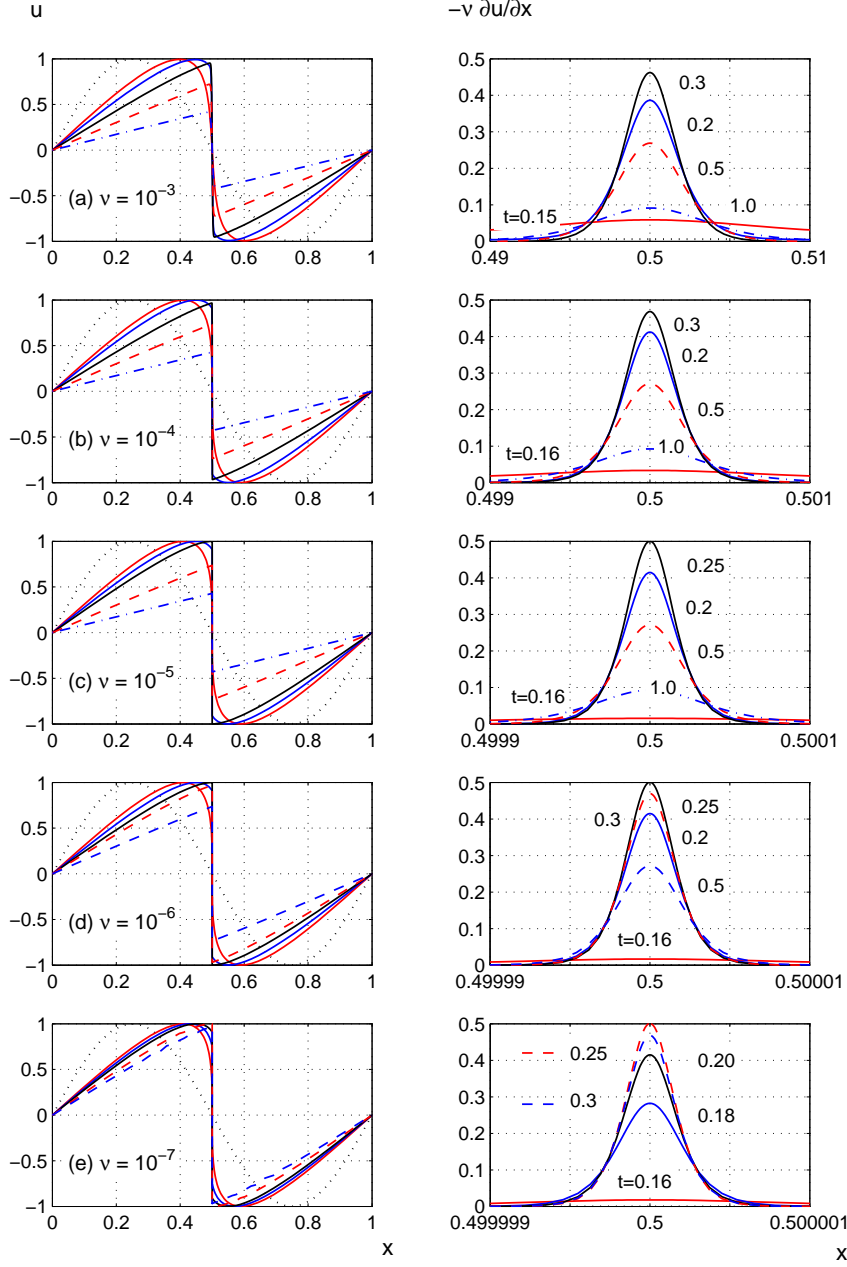


Figure 7. Velocity and vorticity results at various viscosity. Initial data  $u_0(x) = \sin(2\pi x)$ . The temporal resolutions are in the order of  $\nu$ . In each zoom-in view on the right column, there is a sharp increase in the local  $\partial u / \partial x$  from time 0.158 to 0.25 (the transition period). The velocity profiles on the left column display similar evolution characters largely independent of viscosity (for the identical initial data).

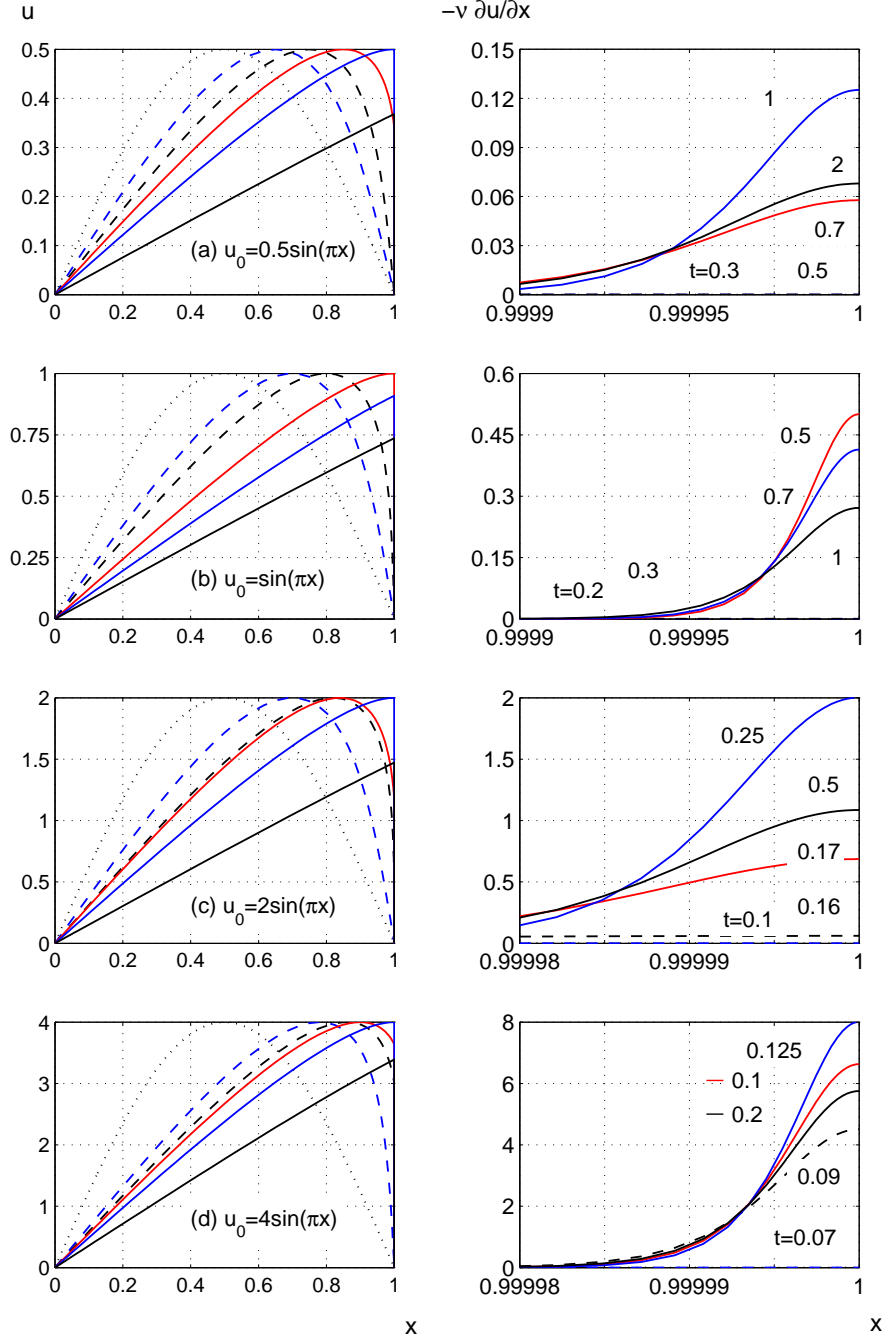


Figure 8. Effect of initial strength,  $\nu = 10^{-5}$ . The intensification begins sooner over narrower space as the initial strength becomes stronger. As labelled, the small-time cases in the right column appear as horizontal lines because their intensities are too weak to be significant on the plotting scales.

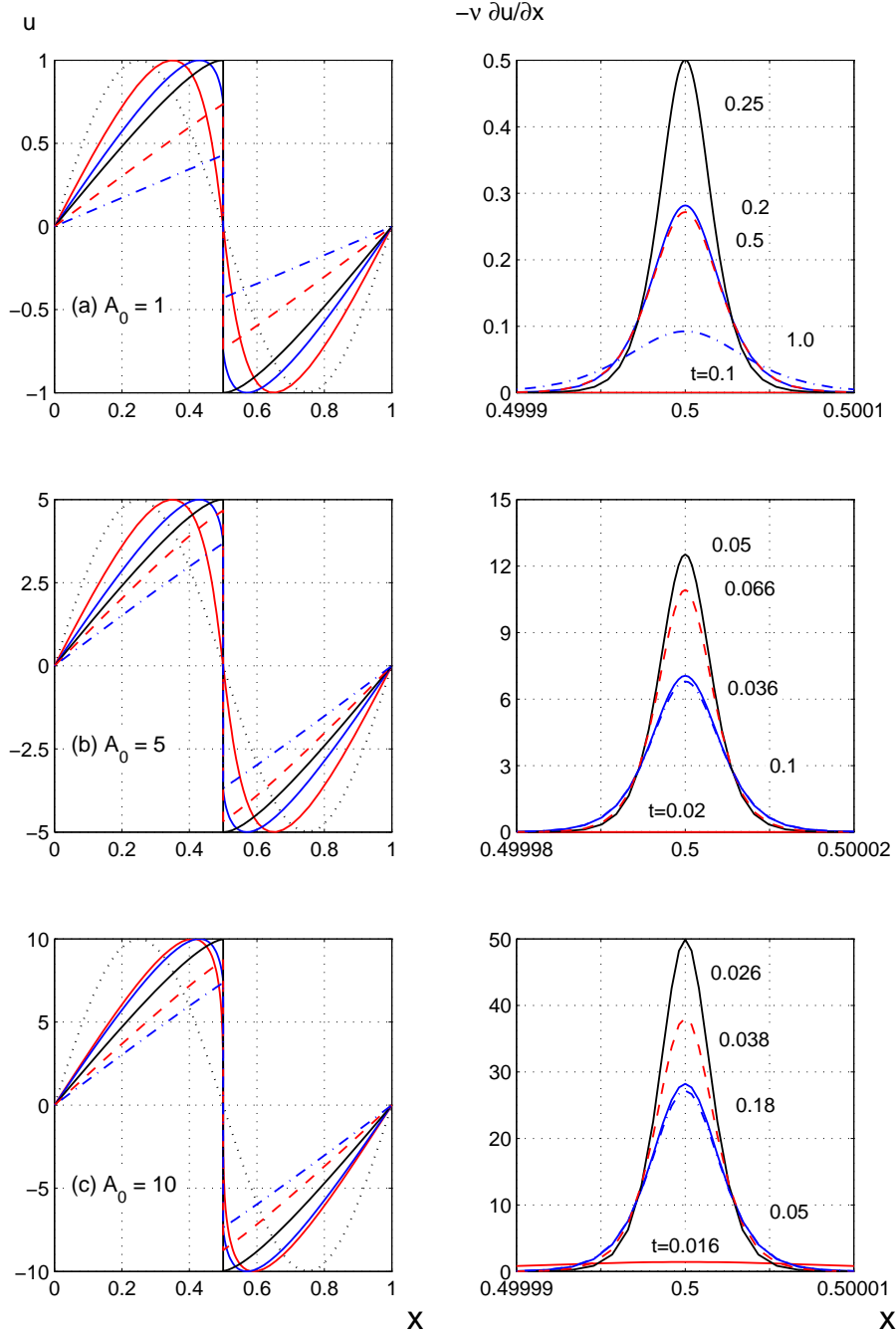


Figure 9. Effect of data size  $u_0(x) = A_0 \sin(2\pi x)$ ,  $\nu = 10^{-5}$ . The shear scaled by viscosity on the right equals to the ‘shear stress’ per unit energy, similar to (2.7). It may be normalised by  $u_0^2/2$  so that, in all the three cases, the maximum shear stress is in the order of unity.



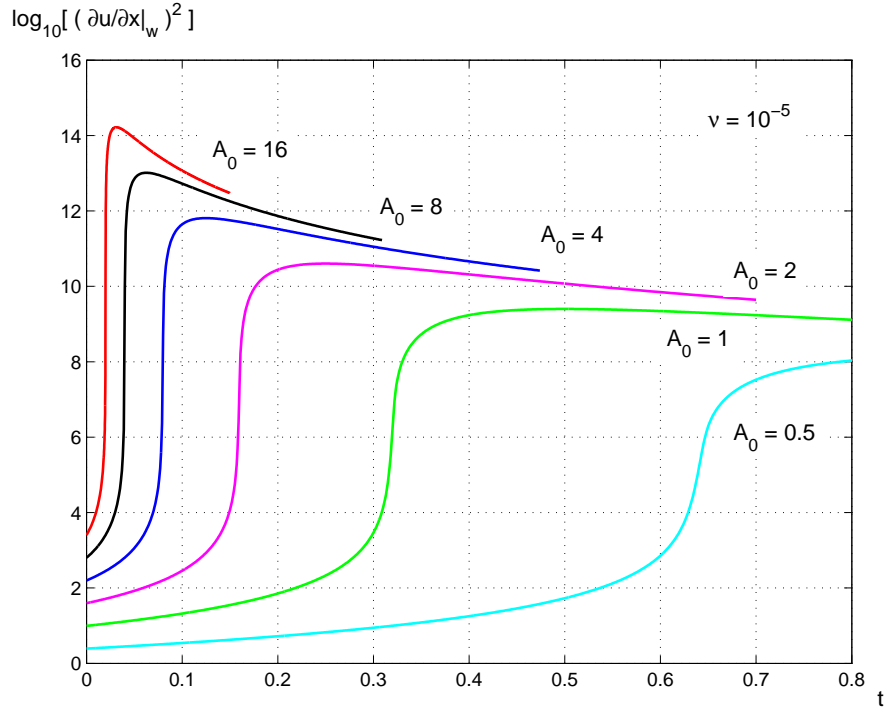


Figure 10. Evolution of wall enstrophy as a function of data size,  $u_0(x) = A_0 \sin(\pi x)$ . For sufficiently large data, there is an *overshoot* just after the intensive non-linear growth, corresponding to a temporary increase in the local turbulent skin friction coefficient. The overshoot phenomenon depends on the size of initial data. As the initial data increase, the initial laminar runs diminish or may even disappear completely. (In higher space dimensions, the vertical jumps are expected to reduce owing to the extra degrees of freedom.) These ‘step-ramps’ are the trademark of the laminar-turbulent transition. In the present figure, time  $t$  may be interpreted as a measure of Reynolds number as  $R_x = xu/\nu \sim tu^2/\nu \propto t$  in time-mean flow. From wind-tunnel experiments, it is known that the local skin friction of turbulent boundary layer settles down on a characteristic function of Reynolds number (cf. Fig. II.25 of Lighthill 1963).

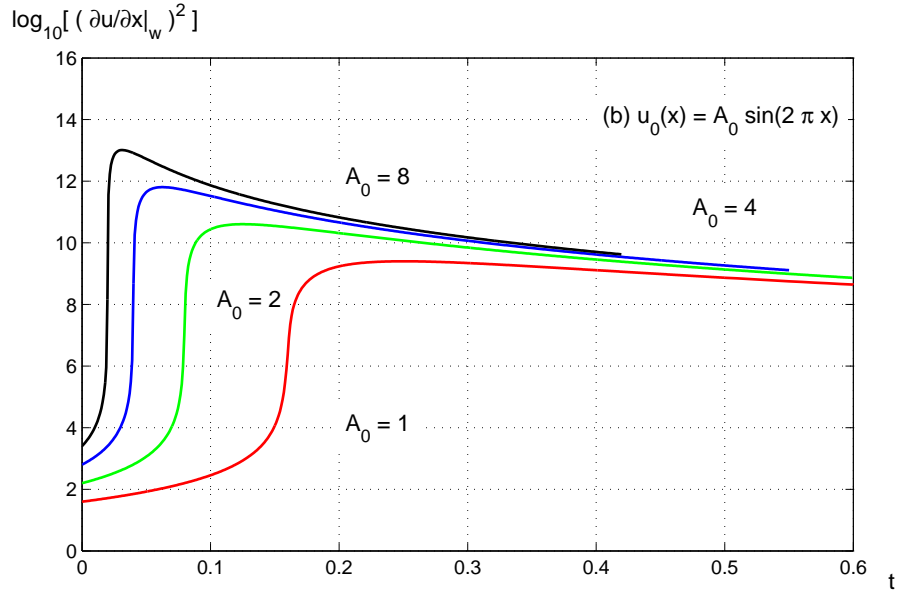
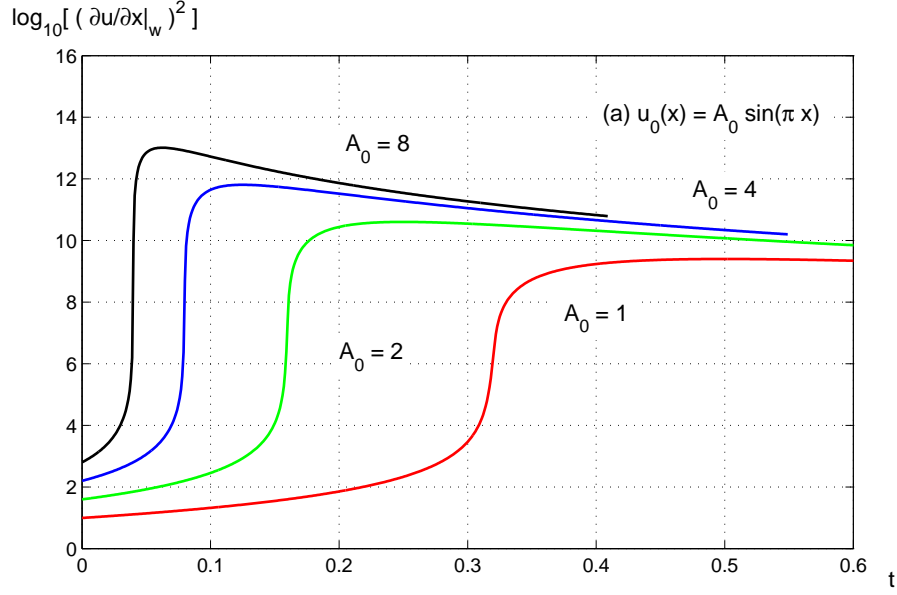


Figure 11. Overshoot in local enstrophy as a genuine feature during flow development. Viscosity  $\nu = 10^{-5}$ . There are well-defined overshoots in either case, particularly in flows of large initial amplitudes. Note that either group of the vorticity soon converges to an identical decay regardless of the initial size.

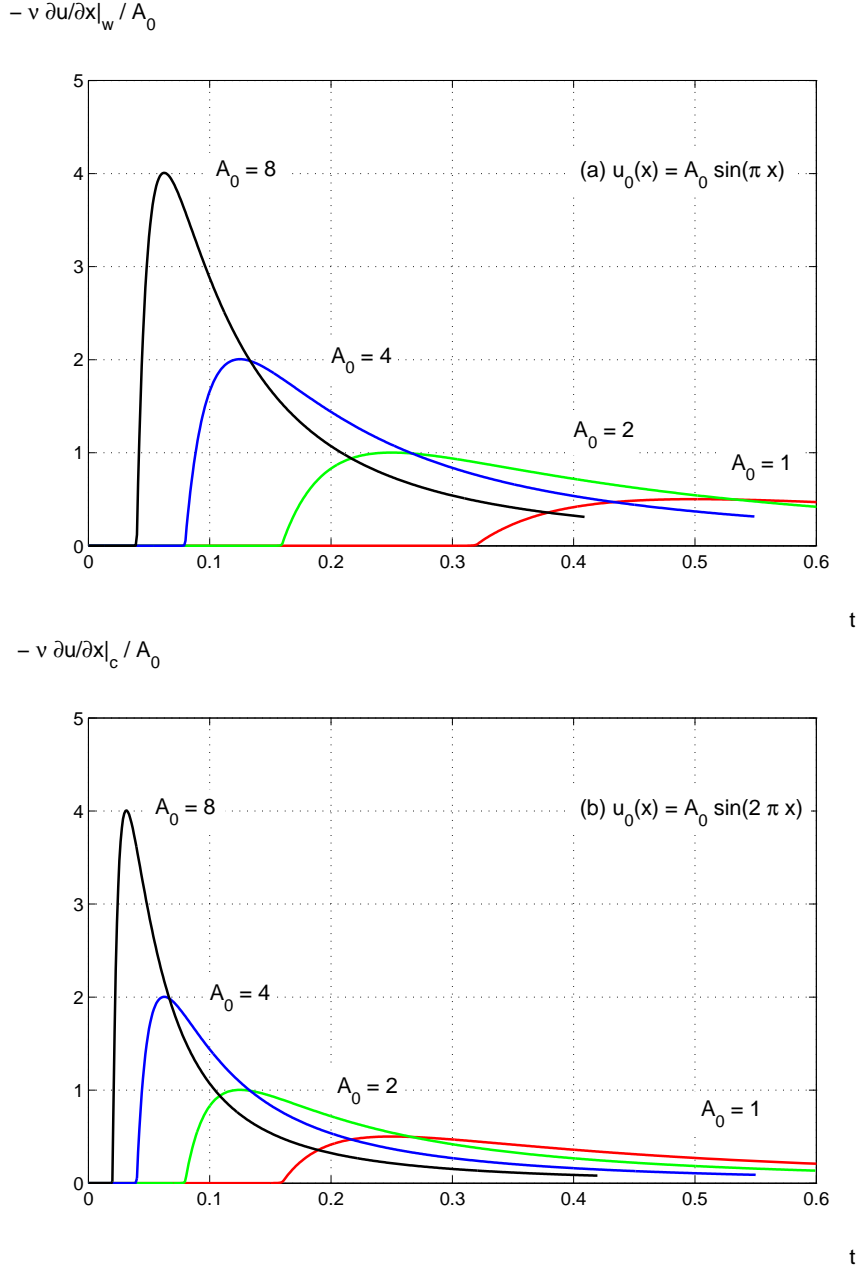


Figure 12. Maximum shear as a function of time,  $\nu = 10^{-5}$ . Over the initial phase (laminar state), the magnitudes of vorticity are increasing with time but they are too small to show up in the vertical scale. In each case of (a), the intensified shear over the abrupt jump resembles the increased skin friction in a typical turbulent flow through the process of the laminar-turbulent transition. Each accumulated shear in (b) has a steeper rise or drop. (In higher space dimensions, this property likely contributes to the diverse topology of vortices commonly existed in high-Reynolds-number free-shear flows.)

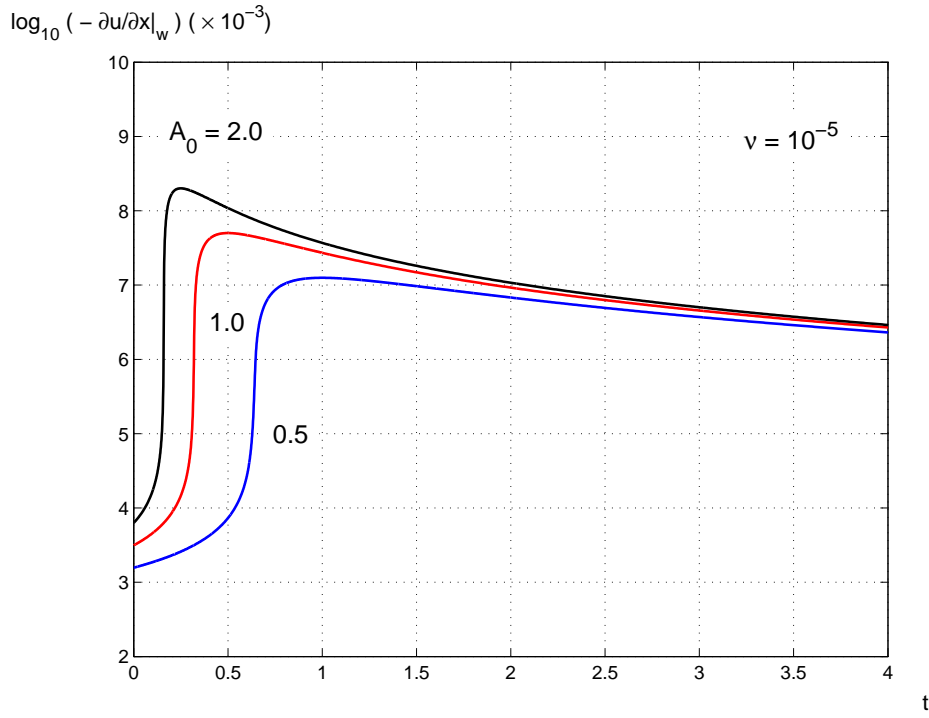


Figure 13. Time decay of wall shear,  $u_0(x) = A_0 \sin(\pi x)$ . The time scale  $t \sim O(1)$  covers the initial period in typical applications. The rate of the wall enstrophy decay flattens out after  $t > 4$  and indeed the turbulent flows are largely history-independent as advocated in theory. Because of the transition, the short-time impact due to the initial data must be consequential in flow control (see also figure 11).

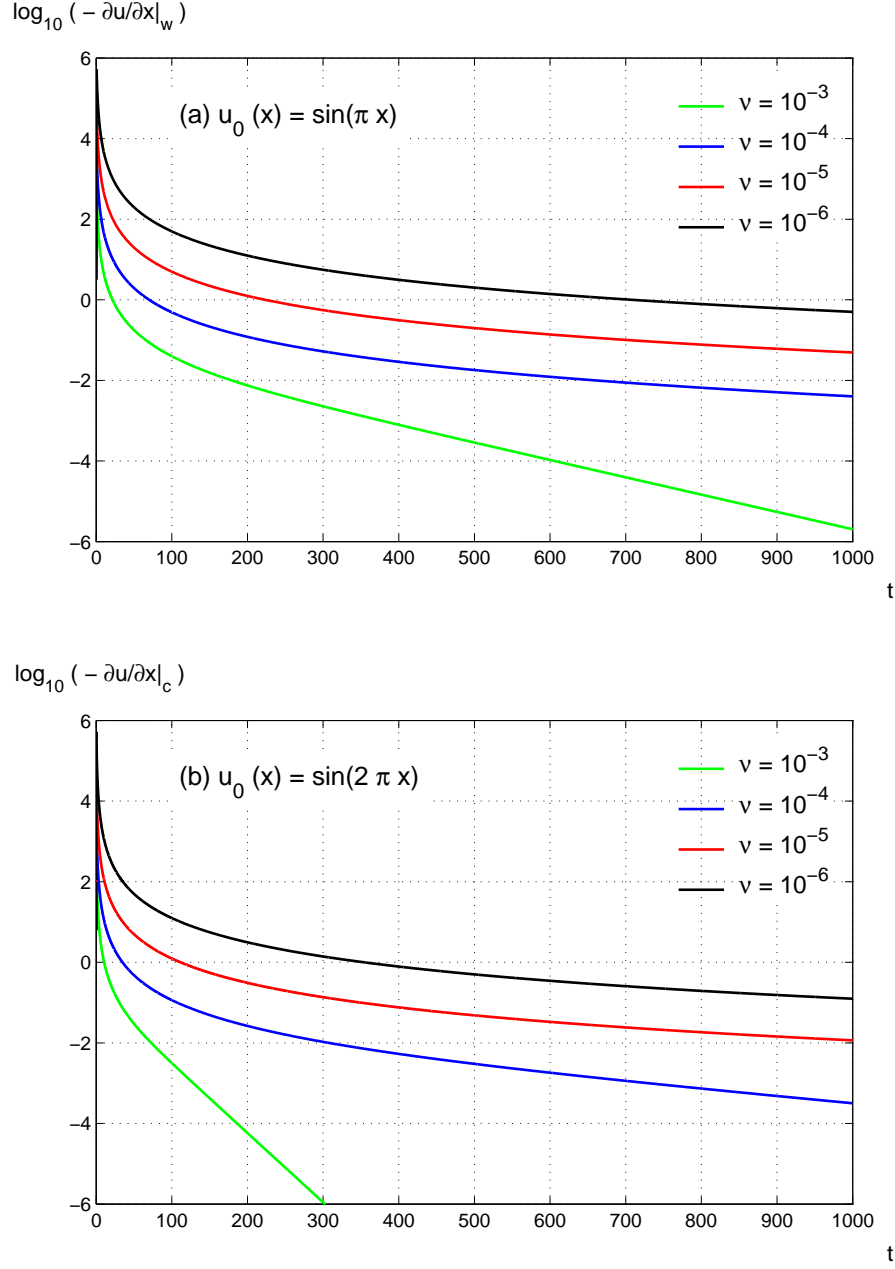


Figure 14. Decay of Burgers turbulence at various values of viscosity. The long-term decay is pretty much identical for the two cases whose initial energies are in the same order of magnitude. The trend in the green lines may be related to the decay of laminar flow.

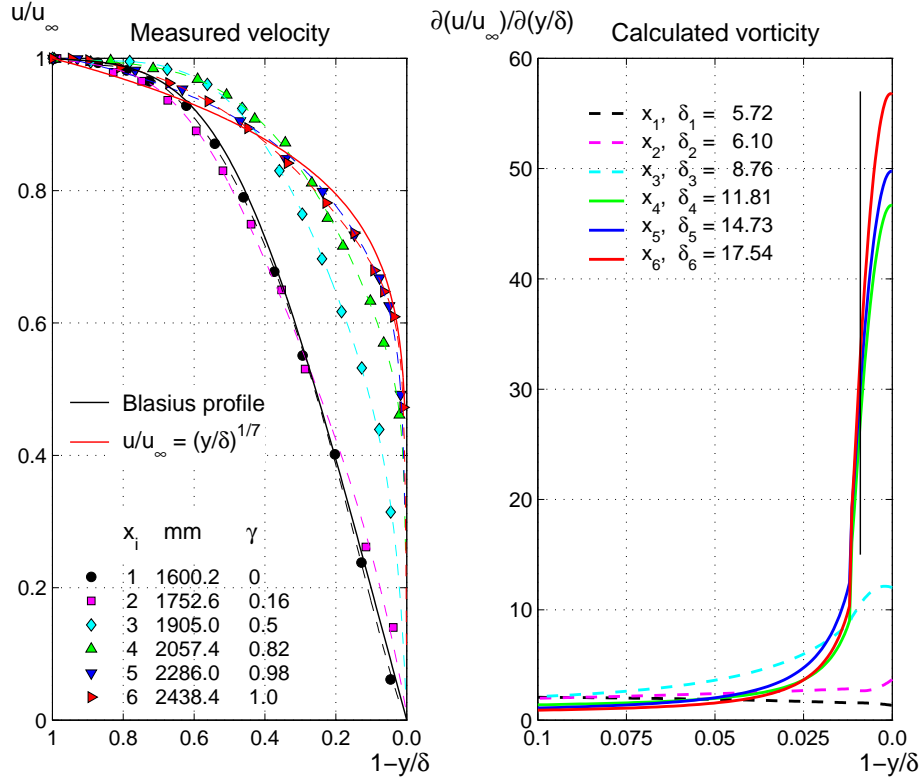


Figure 15. Measured velocity at 6 streamwise stations over the laminar-turbulent transition in a flat-plate boundary layer as presented in figure 3 of Schubauer & Klebanoff (1955). Symbols are the experiment data and lines are best fitted rational functions. The small waviness in the calculated vorticity is largely due to the ‘read-out’ errors from the sparse data points. Position  $x$  is the distance from the leading edge and the values given in the legend are estimated boundary layer thickness  $\delta$  (in mm). The uniform free stream speed was  $u_\infty = 24.38$  m/s and the free stream turbulence level 0.03%. The transition zone covered a length  $\sim 700$  mm. The tests were carried out at normal room conditions (kinematic viscosity  $\nu \approx 1.5 \times 10^{-5}$  m<sup>2</sup>/s). The intermittency factor  $\gamma$  was the measured fraction of the total time that the local flow was turbulent. It took merely 30 ms for the (non-dimensional) vorticity to grow 15 – 20 times from the Blasius state  $x_2$  to station  $x_6$ , taking into account the uncertainty in the wall profile measurements across the transition region; the abrupt shear increase was squeezed into a thin layer of 5 mm above the wall ( $\delta_4$  to  $\delta_6$ ). The unresolved area is indicated by a vertical black line in the vorticity plot corresponding to the first measurement point from the wall. The peak velocity fluctuations were measured in a width of 1.5 mm next to the wall (cf. figure 4 of the test data). Based on the theory presented in fig. II. 25 of Lighthill (1963), the jump in local skin friction  $C_f$  at transition Reynolds number  $3.3 \times 10^6$  is  $\Delta C_f \approx 0.003$  (including the local overshoot) which translates into a vorticity increase of 40 at the end of transition  $x_6$ .

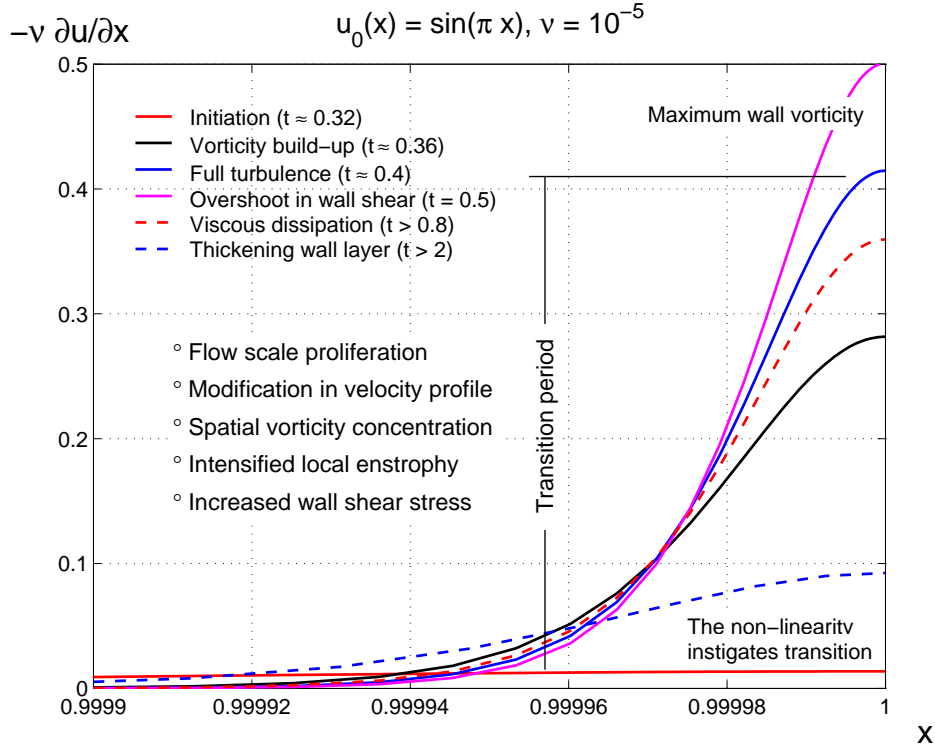


Figure 16. Refer to figure 1. The intense build-up of vorticity at wall between  $t \approx 0.32$  and  $t \approx 0.4$  is the hallmark of the laminar-turbulent transition. The continued shear growth from  $t > 0.4$  to the maximum produces an overshoot in the local ‘skin friction’ due to different rates of vorticity intensification across  $x$ . The state of the flow is fully turbulent as the friction is substantially higher than that before  $t = 0.32$ . The fully-developed turbulence resides in the thin region  $\Delta x \approx \nu$ . In the subsequent decay, the viscous dissipation of the coalesced wall vorticity is largely confined to the wall vicinity  $0.999 \leq x \leq 1$ ; the numerical data show that the maximum vorticity  $|\partial_x u|_{\max} \approx 78, 20, 5$  and  $0.2$  at time  $t = 25, 50, 100$  and  $500$  respectively. As  $t \rightarrow \infty$ , the viscous layer becomes thicker and expands toward the other end  $x = 0$  until the whole region  $0 \leq x \leq 1$  reverts to a quiescent state. At  $t = 2000$ ,  $u_{\max}$  decreases to  $4.4 \times 10^{-4}$  near  $x = 0.9$ , and the vorticity to  $1.2 \times 10^{-2}$  at the wall. The overall shear is reduced to  $5 \times 10^{-4}$  over  $0 \leq x \leq 0.8$ .

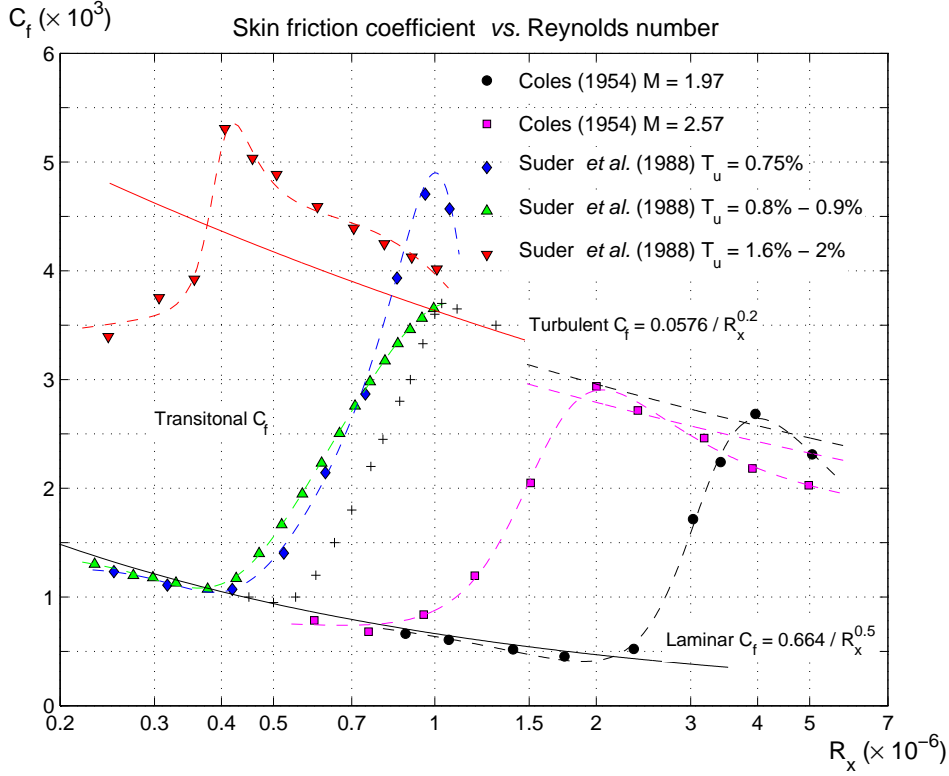


Figure 17. Increase in wall shear from laminar to turbulent state and evidence of overshoots in boundary layer experiments. Skin friction coefficient  $C_f$  is defined as the ratio of wall shear  $\tau_w$  and the free-stream dynamic head  $\rho u_\infty^2/2$ . Reynolds number  $R_x$  is based on the stream-wise distance from the leading edge ( $x$ ). The trend lines are added to the test data for indication only. Coles' data were collected over the natural transition. The  $M=1.97$  data have been shifted by  $-0.1$  for consistency. The grid-produced free-stream turbulence in the data of Suder *et al.* is measured in the fraction of average turbulent fluctuation relative to  $u_\infty$  ( $T_u$ ). This specific experiment deals with distorted transitions. Turbulent skin friction is calculated by assuming a velocity profile of  $u/u_\infty = (y/\delta)^{1/7}$ . The effects of Mach number on the skin friction are estimated and shown in broken curves. Particularly, the influence of the free-stream turbulence on the natural transition was far from clear. The last data set suggests that the lift-span of the laminar boundary layer was rather brief, if ever existed. Nevertheless, each test run highlights a well-marked 'ramp' over the transition though the fully-developed turbulence downstream of the maximum stress behaves somehow differently. It is plausible that the incompressible data are not finely-tuned as the short-term records have to be dominated by the details in respective leading-edge condition. For reference, the trend (+ symbols) is added: it is the flat-plate natural transition starting  $R_x \approx 0.5 \times 10^6$ , estimated from the data in fig.II.25 of Lighthill (1963) and fig.21.2 of Schlichting (1979). The test results can be better understood by comparing with the calculations in figures 10 and 11.